geosciences

MDPI

Article

The Importance of Eurekan Mountains on Cenozoic Sediment Routing on the Western Barents Shelf

Michael J. Flowerdew [1,*], Edward J. Fleming [1,2], David M. Chew [3], Andrew C. Morton [1,4], Dirk Frei [5], Aukje Benedictus [6], Jenny Omma [6], Teal. R. Riley [7], Eszter Badenszki [8] and Martin J. Whitehouse [9]

1 CASP, Madingley Rise, Madingley Road, Cambridge CB3 0UD, UK
2 Mott MacDonald Group Ltd., 22 Station Road, Cambridge CB1 2JD, UK
3 Department of Geology, School of Natural Sciences, Trinity College Dublin, Dublin 2, Ireland
4 Department of Geology and Geophysics, King's College, University of Aberdeen, Aberdeen AB24 3UE, UK
5 Department of Earth Sciences, University of the Western Cape, P/Bag X17, Bellville 7530, South Africa
6 Rocktype, Magdalen Centre, Robert Robinson Avenue, Oxford OX4 4GA, UK
7 British Antarctic Survey, High Cross, Madingley Road, Cambridge CB3 0ET, UK
8 UCD School of Earth Sciences, University College Dublin, Belfield, Dublin 4, Ireland
9 Swedish Museum of Natural History, P.O. Box 50 007, SE-104 05 Stockholm, Sweden
* Correspondence: michael.flowerdew@casp.org.uk

Abstract: The importance of topography generated by Eocene Eurekan deformation as a sediment source for sandstones deposited on the western Barents Shelf margin is evaluated through a sediment provenance study conducted on wellbore materials retrieved from Spitsbergen and from the Vestbakken Volcanic Province and the Sørvestsnaget Basin in the southwest Barents Sea. A variety of complementary techniques record a provenance change across the Paleocene-Eocene boundary in wellbore BH 10-2008, which samples Paleogene strata of the Central Tertiary Basin in Spitsbergen. Sandstones containing K-feldspar with radiogenic Pb isotopic compositions, chrome spinel in the heavy mineral assemblage, and detrital zircons and rutiles with prominent Palaeoproterozoic and Late Palaeozoic—Early Mesozoic U-Pb age populations are up-section replaced by sandstone containing albitic plagioclase feldspar, metasedimentary schist rock fragments, a heavy mineral assemblage with abundant chloritoid, metamorphic apatite with low REE contents, metapelitic rutile with Silurian U-Pb ages and zircons with predominantly Archaean and Palaeoproterozoic U-Pb age populations. Our results clearly demonstrate the well-known regional change in source area from an exposed Barents Shelf terrain east of the Central Tertiary Basin during the Paleocene to the emerging Eurekan mountains west and north of the Central Tertiary Basin during the Eocene. Eocene sandstones deposited in the marginal basins of the southwestern Barents Shelf, which were sampled in wellbores 7316/5-1 and 7216/11-1S, contain elements of both the Eurekan and the eastern Barents Shelf provenance signatures. The mixing of the two sand types and delivery to the southwest margin of the Barents Shelf is consistent with a fill and spill model for the Central Teritary Basin, with transport of Eurekan-derived sediment east then south hundreds of kilometres across the Shelf.

Keywords: source-to-sink; sediment provenance; Eocene; Paleogene; Spitsbergen fold-and-thrust belt; Central Tertiary Basin; Torsk Formation

Citation: Flowerdew, M.J.; Fleming, E.J.; Chew, D.M.; Morton, A.C.; Frei, D.; Benedictus, A.; Omma, J.; Riley, T.R.; Badenszki, E.; Whitehouse, M.J. The Importance of Eurekan Mountains on Cenozoic Sediment Routing on the Western Barents Shelf. *Geosciences* **2023**, *13*, 91. https://doi.org/10.3390/geosciences13030091

Academic Editors: Salvatore Critelli and Jesus Martinez-Frias

Received: 20 December 2022
Revised: 10 March 2023
Accepted: 16 March 2023
Published: 21 March 2023

1. Introduction

Eocene Eurekan deformation, caused by the anti-clockwise rotation of Greenland and its oblique collision with neighbouring plates [1], is manifest by the development of fold-and-thrust belts on the Canadian Arctic islands, in north Greenland and along west Spitsbergen. The deformation is estimated to have, in places, driven over 8 km of exhumation, extensive shortening and the widespread development of substantial topography [2–4]. The Eurekan deformation zone, with an extensive fold-and-thrust belt

centred over the Ellesmere Island and extending to north Greenland and west Spitsbergen (Figure 1), was therefore likely to be a substantial sediment factory throughout the Eocene.

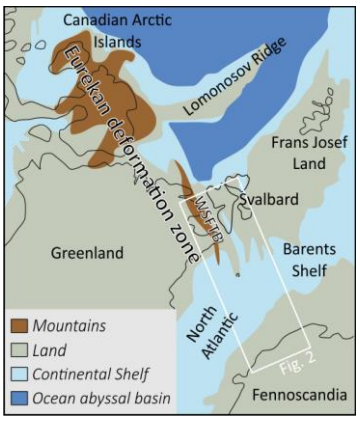

Figure 1. Eocene palaeogeography reconstruction showing the extent of the Eurekan relief after Blakey [4] and Smelror, et al. [5]. WSFTB = West Spitsbergen fold-and-thrust Belt. The location of the study site and region covered by Figure 2 is indicated.

The development of the Central Tertiary Basin on Spitsbergen was intrinsically linked with the early Eocene phase of the Eurekan deformation [6–8], which resulted in the formation of the West Spitsbergen fold-and-thrust belt [8–10]. During the Eocene, the Central Tertiary Basin was predominantly filled by material eroded from the emerging West Spitsbergen fold-and-thrust belt highlands [11] and so was an important sediment sink. This flexural basin was strongly asymmetric, meaning that subsidence was lower along its eastern margin where deposition was initially dominated by coastal plain environments [12] and clastic input from a forebulge located to the east of the basin [10,13], in addition to material sourced from the West Spitsbergen fold-and-thrust belt and transported via longshore drift [12]. At its western margin, rapid subsidence over-deepened the basin and sediment was initially supplied via submarine fans [14]. Subsequently, sediment supply largely kept pace or exceeded subsidence during the progressive infilling of the basin with the stacking and progradation of clinoform sequences preserving deltaic, shelf, slope and basin floor facies, as well a as thick continental succession [9,11,15].

Palaeoflow indicators on Spitsbergen indicate a strong component of sediment transport from west to east [11], cognate with the architecture and progradation of clinoform sequences [9,14]. A western, proximal and immature source for the sediment is supported by detrital zircon U-Pb geochronology [16] and by sandstone textural and petrographic information [11,17]. The thickest stratigraphy occurs at the southern-most exposure of the basin on Spitsbergen [9], which raises the possibility that clastic material spilled south and east onto the Barents Shelf. Seismic interpretations indicate that large volumes of sediment were deposited on the southwest Barents Shelf margin synchronously with those within the Tertiary Central Basin but 300 km farther south of Spitsbergen [18,19]. These sedimentary units are argued to either have a northerly source, from the proximal and adjacent structural highs [18,20] that were possibly affected by deformation relating to the West Spitsbergen fold-and-thrust belt [21], or from northern Fennoscandia [22]. Whilst it is tempting to link the source of this sediment to the West Spitsbergen fold-and-thrust belt situated to the north where palaeoelevations and sediment production rates were high [2,5], evidence for coupling of the sediment delivered to the Central Tertiary Basin and that to the southwest Barents Shelf system is lacking and remains speculative [9]. Although plausible, sediment routing probably required a significant easterly diversion en-route from south to north. Synchronous with the Eocene transpressive regime on Spitsbergen was a phase of transtensional tectonism in the vicinity of the southwest Barents Shelf [23,24]. A series of pull-apart basins developed during this Eocene phase of extension [25], within which the silt-dominated Torsk Formation sediments accumulated [20].

This sediment provenance study aims to test whether or not sediments derived from the West Spitsbergen fold-and-thrust belt eventually bypassed the Central Tertiary Basin to be deposited in basins along the margin of the southwest Barents Shelf. We use a multitude of complementary techniques to investigate and compare Eocene samples of the Torsk Formation collected from two exploration wells on the southwest Barents Shelf with samples from the Paleocene to Eocene from Van Meijfjorden Group in the Central Tertiary Basin collected from wellbore BH 10-2008 onshore Spitsbergen (Figure 2). We further discuss our results in the larger framework of previous provenance interpretations [8,11,16]. Finally, we provide greater clarity on early Cenozoic sediment routing by identifying sedimentary reworking and natural biases that may otherwise skew sediment dispersal models, e.g., [26,27].

2. Geological Background

The Central Tertiary Basin comprises approximately 2300 m of stratigraphy formed of six formations collectively termed the Van Meijfjorden Group [28] and is exposed in southern Spitsbergen (Figure 2). It formerly had a greater extent but substantial post-depositional uplift [29] caused only small outliers to remain in northern Spitsbergen [30]. Subsidence and basin development started during the Paleocene in relation to the evolving west Spitsbergen fold-and-thrust Belt, when the Firkanten Formation was deposited unconformably on Albian strata. Initial sedimentation occurred within coastal plain and shallow marine environments and is associated with coal deposits in central Spitsbergen [12]. The Paleocene Firkanten and subsequent marine mudstone-dominated Basilika and shelfal sandstone-dominated Grumantbyen formations had sources located north and east of the Central Tertiary Basin based on field and petrographic observations [11]. Additional sediment provenance, geochemical and reworked palynomorph data also indicate that the sediment source region was located to the east on the Barents Shelf and it comprised predominantly Mesozoic strata [13,16,31–33], data that is consistent with seismic interpretations [34].

The developing topography within the Eurekan deformation zone caused a sediment provenance switch, an increase in textural and compositional immaturity and basin deepening as a response to flexural loading [9,17]. Sandy units within the Frysjaodden Formation represent basin floor fans emplaced by sediment gravity flows with inferred West Spitsbergen fold-and-thrust belt sources located to the west [14]. Plink-Björklund et al. [35] determined that delivery of sand across the shelf onto basin floor resulted from hyperpycnal flows associated with fluvial-deltaic systems at the basin margins, possibly triggered by storm events. Evidence for extreme climatic excursions are also recorded within the Frysjaodden Formation and these are associated with the Paleocene-Eocene boundary, which is constrained to *c.* 55.9 Ma on Spitsbergen [36]. The later Eocene sandstone-dominated Battfjellet and heterolithic Aspelintoppen formations were deposited in stacked shallow marine, deltaic and coastal plain clinothems that prograded from west to east and had sources from the west [16]. The west sediment source region and Eurekan deformation zone encompasses a diverse suite of rocks. In north Greenland, the terrain is predominantly Early Palaeozoic carbonates and clastic strata derived from the Greenland craton and metamorphosed during the Late Devonian Ellesmerian tectonism. The geology proximal to the basin margin differs from that of north Greenland. Here, predominantly Neoproterozoic strata have been variably affected by Late Neoproterozoic "Timanian" and Ordovician-Silurian Caledonian events in addition to Late Devonian "Svalbardian" or Ellesmerian deformation [37]. Perhaps the strongest and most distinctive of these is the Caledonian, where blueschist metamorphic assemblages [38] and widespread migmatisation and granitoid intrusion are recorded [39]. However, rocks affected by amphibolite-facies Ellesmerian metamorphism are reported from the Pinkie Unit on Prins Karls Forland [40].

A thick sedimentary succession was deposited within pull-apart basins [23,24] at the southwest margin of the Barents Shelf, synchronously with the Van Meijfjorden Group in Central Tertiary Basin on Spitsbergen. This succession is in its entirety assigned to the sandstone-poor Torsk Formation. During the early Eocene, however, greater volumes of

sediment were supplied to these basins [41] including some sands emplaced by sediment gravity flows and reworked by bottom currents [20]. Within the Vestbakken Volcanic Province and Sørvestsnaget Basin, south-prograding clinoform and submarine fan systems deposited over 2000 m of strata [18,20,42], which had sources from the Barents Shelf, including the proximal Stappen and Loppa structural highs [19,20]. Mesozoic sedimentary rocks reworked from the Stappen high and northern parts of the Barents Shelf would likely have delivered different provenance signals to the Torsk basins than sedimentary rocks reworked from the Loppa High and southern parts of the Barents Shelf. This is because Cretaceous strata deposited on the Stappen High were sourced from large prograding systems from the north, and these systems did not reach the Loppa High and southern most regions [43,44]. Similarly, the Triassic and Jurassic strata probably also had contrasting provenance in the north and the south regions of the Barents Shelf. In the south, a greater influence from Fennoscandia is evident and zircon age spectra suggest that some easterly-sourced Triassic had a different Uralian Orogenic source compared with Triassic deposited father north [27,45–48].

3. Materials and Methods

A total of 28 samples were investigated, which came from three wellbores on Svalbard and the southwest margin of the Barents Shelf. Research well BH 10-2008 was drilled near the axis of the Central Tertiary Basin onshore Spitsbergen at Sysselmannbreen [49] and a continuous cored section was retrieved through large parts of the Van Mijenfjorden Group (Figure 2). Two exploration wells 7316/5-1 and 7216/11-1S were drilled in the Vestbakken Volcanic Province and Sørvestsnaget Basin (Figure 2). Wellbore materials may be viewed at the Norwegian Petroleum Directorate. The samples weigh between 40 and 50 g. Thirteen sandstone samples are from the Paleogene strata of the Central Tertiary Basin, whereas the remaining 15 sandstone and siltstone samples from the Vestbakken Volcanic Province and the Sørvestsnaget Basin on the southwest Barents Shelf. Figure 2 and Table 1 detail the sample locations and the techniques applied to the samples.

Table 1. Sample and analysis information.

Sample	Lat [1]	Long [2]	Formation	Unit	Petrog [3]	HMA [4]	QS [5]	Kfs Pb	Apatite U-Pb/Chem	Rutile U-Pb/ Chem	Zircon U-Pb
BH 10-2008 51.98	77.630	16.027	Aspelintoppen	3B	•	•	•				
BH 10-2008 98.00	77.630	16.027	Battfjellet	3A	•	•	•				
BH 10-2008 137.90	77.630	16.027	Battfjellet	3A	•		•	•	•	•	•
BH 10-2008 290.92	77.630	16.027	Frysjaodden	2	•	•					
BH 10-2008 332.96	77.630	16.027	Frysjaodden	2	•	•	•				
BH 10-2008 356.00	77.630	16.027	Frysjaodden	2	•	•	•				
BH 10-2008 375.00	77.630	16.027	Frysjaodden	2	•		•	•	•	•	•
BH 10-2008 387.96	77.630	16.027	Frysjaodden	2	•	•	•				
BH 10-2008 417.06	77.630	16.027	Frysjaodden	2	•	•	•				
BH 10-2008 427.63	77.630	16.027	Frysjaodden	2	•	•	•				
BH 10-2008 840.00	77.630	16.027	Grumantbyen	1	•	•	•				
BH 10 2008-871.90	77.630	16.027	Grumantbyen	1	•		•	•		•	•
BH 10-2008 895.00	77.630	16.027	Grumantbyen	1	•	•	•				
7316/5-1 1353.10	73.520	16.431	Torsk	B	•	•					
7316/5-1 1353.40	73.520	16.431	Torsk	B		•					
7316/5-1 1359.50	73.520	16.431	Torsk	B	•	•					
7316/5-1 1364.80	73.520	16.431	Torsk	B		•					
7316/5-1 1370.30	73.520	16.431	Torsk	B		•					
7316/5-1 1373.20	73.520	16.431	Torsk	B	•	•					
7316/5-1 1373.70	73.520	16.431	Torsk	B		•					

Table 1. *Cont.*

Sample	Lat [1]	Long [2]	Formation	Unit	Petrog [3]	HMA [4]	QS [5]	Kfs Pb	Apatite U-Pb/Chem	Rutile U-Pb/ Chem	Zircon U-Pb
7316/5-1 1464.50	73.520	16.431	Torsk	B	•	•		•		•	•
7316/5-1 1467.10	73.520	16.431	Torsk	B	•	•					•
7316/5-1 1468.40	73.520	16.431	Torsk	B	•	•				•	
7316/5-1 1469.80	73.520	16.431	Torsk	B		•					
7216/11-1S 2988.30	72.016	16.604	Torsk	A	•	•					
7216/11-1S 2989.80	72.016	16.604	Torsk	A	•	•		•		•	•
7216/11-1S 2991.30	72.016	16.604	Torsk	A	•	•					
7216/11-1S 2992.90	72.016	16.604	Torsk	A	•	•					

[1] Latitude, [2] Longitude, [3] Petrography, [4] Heavy mineral analysis, [5] QEMSCAN. • indicates that the technique was applied to the sample.

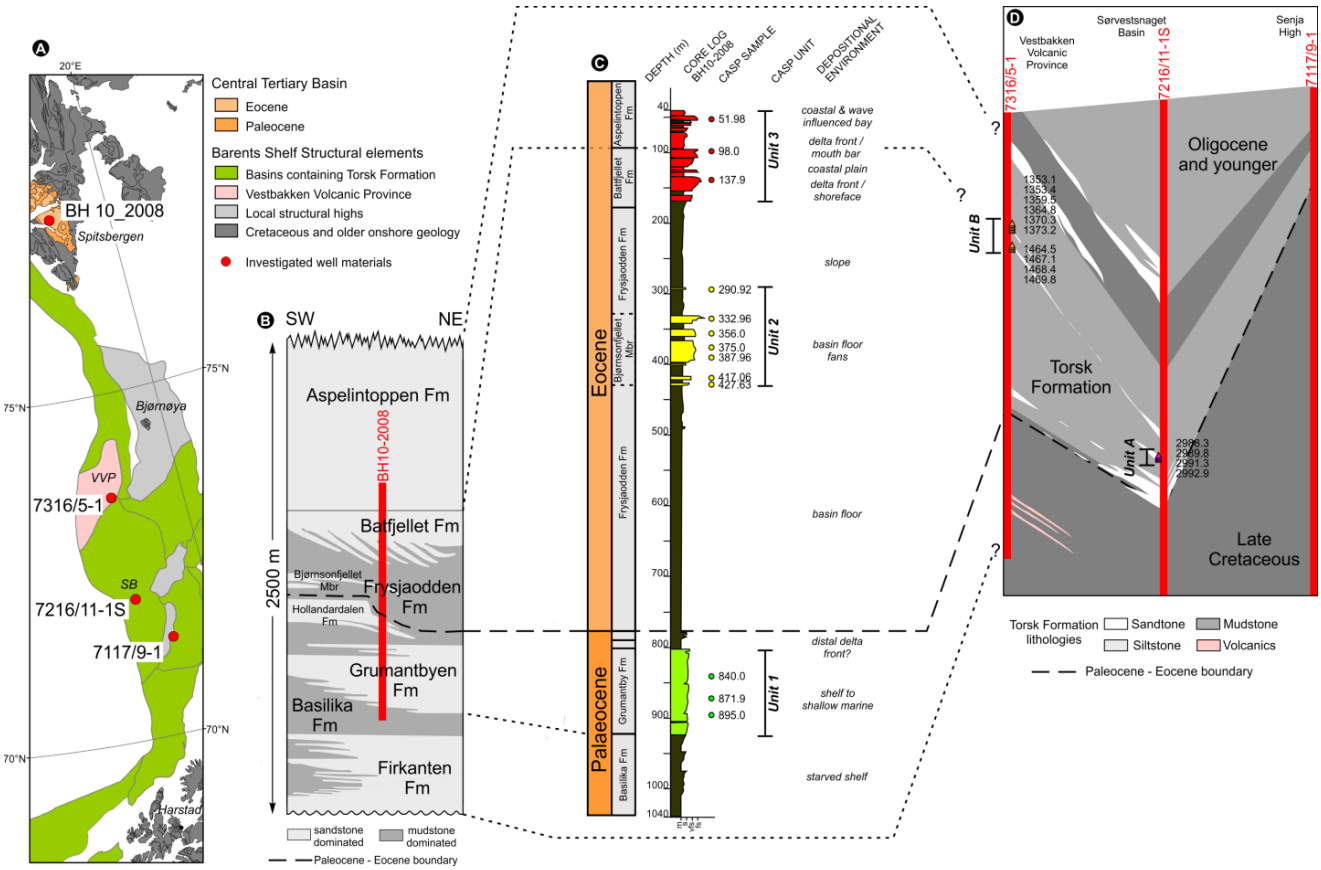

Figure 2. Location and stratigraphy for the investigated samples. (**A**) Map of well locations, relevant structural elements and Central Tertiary Basin outcrop. The Barents Shelf structural elements after Gabrielsen et al. [50] are abbreviated as follows: LH = Loppa High, SB = Sørvestsnaget Basin, SH = Stappen High, VVP = Vestbakken Volcanic Province. (**B**) Central Tertiary Basin stratigraphic cross section adapted from Steel, Dalland, Kalgraff and Larsen [6] shows the BH 10-2008 cored interval. (**C**) Stratigraphic log for well BH 10-2008 after Grundvåg, Johannessen, Helland-Hansen and Plink-Björklund [14], showing the sandstone units and sample locations. (**D**) Torsk Formation cross sections are adapted Ryseth, Augustson, Charnock, Haugerud, Knutsen, Midbøe, Opsal and Sundsbø [20] and Omosanya et al. [51] show the sandstone units and sample locations. The numbers adjacent to the sample symbol indicate the well depth in metres.

Owing to BH 10-2008 wellbore position near the centre of the basin, the section is mud-dominated but contains three separate sandstone packages, henceforth referred to

as units in this paper. The sedimentology of the core is described in detail by Grundvåg, Johannessen, Helland-Hansen and Plink-Björklund [14] and is briefly summarised in Figure 2. Unit 1 sandstones are assigned to the Paleocene Grumantbyen Formation, Unit 2 sandstone-dominated sediments are assigned to the Eocene Frysjaodden Formation and Unit 3 sandstones are assigned to the Battfjellet Formation and lowest-most part of the Aspelintoppen Formation.

Of the thirteen sandstones collected from the BH 10-2008 core (Figure 2), three came from the inferred easterly-sourced shallow marine sandstones of the Grumantbyen Formation (Unit 1), six from the westerly-sourced basin floor fans of the Bjørnsonfjellet Member of the Frysjaodden Formation (Unit 2), two from the westerly-sourced shallow marine-deltaic sandstones of the Battfjellet Formation (Unit 3A), and a single sample from the stratigraphically highest cored sandstone of the Aspelintoppen Formation (Unit 3B).

Exploration wells 7316/5-1 and 7216/11-1S penetrate the south-prograding clinoform and submarine fan system that was deposited on the southwest Barents Shelf within the Vestbakken Volcanic Province and Sørvestsnaget Basin.

Materials from wellbore 7316/5-1 came from two Middle Eocene sandy intervals whereas the single sandy interval sampled from wellbore 7216/11-1S (Figure 2) is also Middle Eocene but older than those collected from 7316/5-1 [51]. For the purposes of this study, the 7216/11-1S materials are termed Unit A, whereas the 7316/5-1 materials are termed Unit B.

The sample information and details of which analytical techniques were conducted on which samples are given in Table 1. The analytical methods are briefly described but further information can be found along with the full data tables with the online Supplementary Materials.

Thin sections were stained for K-feldspar. Point counting was performed using the 'traditional' rather than the Gazzi-Dickinson method; see [52]. The results of this method are a complex function of provenance, transport history and modifications during and after deposition. This is because grains comprising >10% by area of other mineral(s) are considered rock fragments. The plotting position any sample is thus dependent on grain size. A total of 300 individual grains were counted for each section. Rock classifications follow that described by Folk et al. [53].

Disaggregated samples were wet sieved through the 125 and 63 µm sieves, and the resulting >125 µm and 63–125 µm fractions were dried in an oven at 80 °C. The 63–125 µm fraction was placed in bromoform with a measured specific gravity of 2.8. Heavy minerals were allowed to separate under gravity, with frequent stirring to ensure complete separation. The heavy mineral residues were mounted under Canada Balsam for optical study using a polarising microscope. The use of the sieved fraction to calculate heavy mineral indices minimises hydrodynamic sorting effects and so may be utilised to evaluate provenance [54].

SEM-derived automated mineralogy was acquired using the QEMSCAN® platform collected by Rocktype Ltd. The scanning electron microscope (SEM) has backscatter electron (BSE) and energy dispersive X-ray (EDS) detectors to provide automated petrographic quantification of geological samples in the form of spatially resolved compositional and textural data. In this study, all data were collected using a QEMSCAN® WellSite instrument (Aspex Extreme Scanning Electron Microscope with 5030 Bruker EDS detectors) using the FieldScan mode at 15 kV beam energy and 5 µm or 10 µm step intervals. The mineral data were processed in FEI's iDiscover software package using an in-house mineral library developed by Rocktype Ltd.

Lead isotopic analyses of K-feldspar were carried out at the National Centre for Isotope Geochemistry, UCD School of Earth Sciences, University College Dublin and closely followed the procedure outlined by Tyrrell et al. [55] and Flowerdew et al. [56]. Polished sections were imaged by SEM to locate fresh K-feldspar prior to isotopic analysis using a Thermo Scientific Neptune MC-ICP-MS, coupled with a New Wave 193 nm Excimer laser ablation system. In order to aid statistical comparison of the K-feldspar data, single stage model ages are calculated for each analysis, after Stacey and Kramers (1975).

Unsieved fractions of apatite, rutile and zircon were picked from concentrates and mounted in epoxy, polished to half-thickness to expose the grain interiors and imaged by SEM prior to analysis. Zircon, rutile and apatite samples from wellbore BH 10-2008 were analysed at the Department of Geology, Trinity College Dublin, Ireland, closely following the method of Chew et al. [57] using a Photon Machines Analyte Excite 193 nm Excimer UV-laser fitted with a two-volume HelEx cell coupled to a Thermo Scientific iCAP Qs ICP-MS. Zircon data are uncorrected for common lead, and correction for common Pb for the apatite and rutile analyses followed the ^{207}Pb method outlined by Chew et al. [58], using iterative age estimates and the model of Stacey and Kramers [59]. The primary zircon reference material used was the 91,500 standard with a ^{206}Pb/^{238}U TIMS age of 1065.4 ± 0.6 Ma [60]. Subsidiary 337.13 ± 0.37 Ma Plešovice zircon [61] and 416.8 ± 1.3 Ma Temora 2 zircon [62] reference materials were used to monitor reproducibility and accuracy. The *c*. 1.09 Ga R10 rutile [63] was used as the primary rutile reference material with 489.5 ± 0.9 Ma R19b [64] used as a secondary standard. The 473.5 ± 0.7 Ma Madagascar apatite [65,66] was used as the primary apatite reference material, whereas secondary standards comprised the 525.3 ± 1.7 Ma (total Pb/U isochron age;) [67] McClure Mountains apatite and the 32.683 ± 0.050 Ma (linear 3-D isochron age) [68] Durango apatite.

The zircon and rutile analyses from the Torsk Formation samples were carried out at the Central Analytical Facility, Stellenbosch University, South Africa and followed closely the method of Frei and Gerdes [69]. The samples were introduced into either an ESI/New Wave Research, UP213, Nd:YAG laser fitted with a custom low-volume cell (zircon) or an ASI Resolution S155, ArF Excimer Coherent CompexPro 110 with a HelEx large dual volume cell (rutile) coupled to a Thermo Finnigan Element2 single collector HR-SF-ICP-MS. Common Pb was monitored and corrected for using the ^{204}Pb method and the Stacey and Kramers [59] composition at the projected age of the grain for the zircon. The *c*. 609 Ma GJ-1 zircon [70] was used as the primary standard. Secondary zircon standards comprised the 524.36 ± 0.16 Ma M257 zircon [71] and the 337.13 ± 0.37 Ma Plešovice zircon [61]. The *c*. 2.0 Ga SRQ36 rutile [72] and the *c*. 1.09 Ga R10 rutile [63] were used as primary and secondary rutile standards, respectively.

The zircon U-Pb analysis for a single Torsk Formation sample (7316/5-1 1467.1 m) used the CAMECA 1280 ion microprobe at the NORDSIMS facility housed at the Swedish Natural History Museum, Stockholm. The method differs from that reported by Whitehouse and Kamber [73] insomuch that the oxygen ion primary beam was generated using a high-brightness, radiofrequency (RF) plasma ion source (Oregon Physics, Hyperion II, rather than a duoplasmatron) and a focused beam instead of illuminated aperture, as described by Riley et al. [74]. The power law relationship ^{206}Pb/^{238}U^{16}O measured from the 1065.4 ± 0.6 Ma Geostandards 91,500 zircon with U and Pb concentrations of 80 ppm and 15 ppm, respectively [60], was used to calibrate U/Pb ratios following Jeon and Whitehouse [75] and M257 was used as a secondary reference material [76]. Common Pb corrections were applied to analyses where statistically significant ^{204}Pb was detected, using the present-day terrestrial estimate reported by Stacey and Kramers [59].

Trace element compositions were collected concurrently with the apatite and rutile U-Pb data. For rutile, Cr and Nb contents were used to determine if the rutile crystallised within metapelitic or metamafic rocks after Meinhold [77], while the Zr in rutile geothermometer of Watson et al. [78] was used to calculate the rutile crystallisation temperature. For apatite, the Mn, Sr, Th and REE contents were used to distinguish silicic from mafic protoliths, and also rocks affected by low-grade metamorphism, after Morton and Yaxley [79] and O'Sullivan et al. [80].

4. Results

4.1. Central Tertiary Basin—Unit 1, Grumantbyen Formation

This unit is characterised by well-sorted, highly compacted, very fine-grained lithic arkoses (Figure 3). The most distinctive features of these sandstones are the abundant glauconite, feldspar (with plagioclase more common than K-feldspar), and the dominance

of sedimentary and chert rock fragments. The heavy mineral assemblage comprises primarily apatite and the stable minerals rutile, tourmaline and zircon (Figure 4). Calculated provenance sensitive heavy mineral indices yield high ATi values, moderate RuZi values, low GZi values, and CZi values of zero, owing to the absence of chrome spinel (Figure 5). However, some of these values should be treated with caution owing to the low heavy mineral yield for these samples.

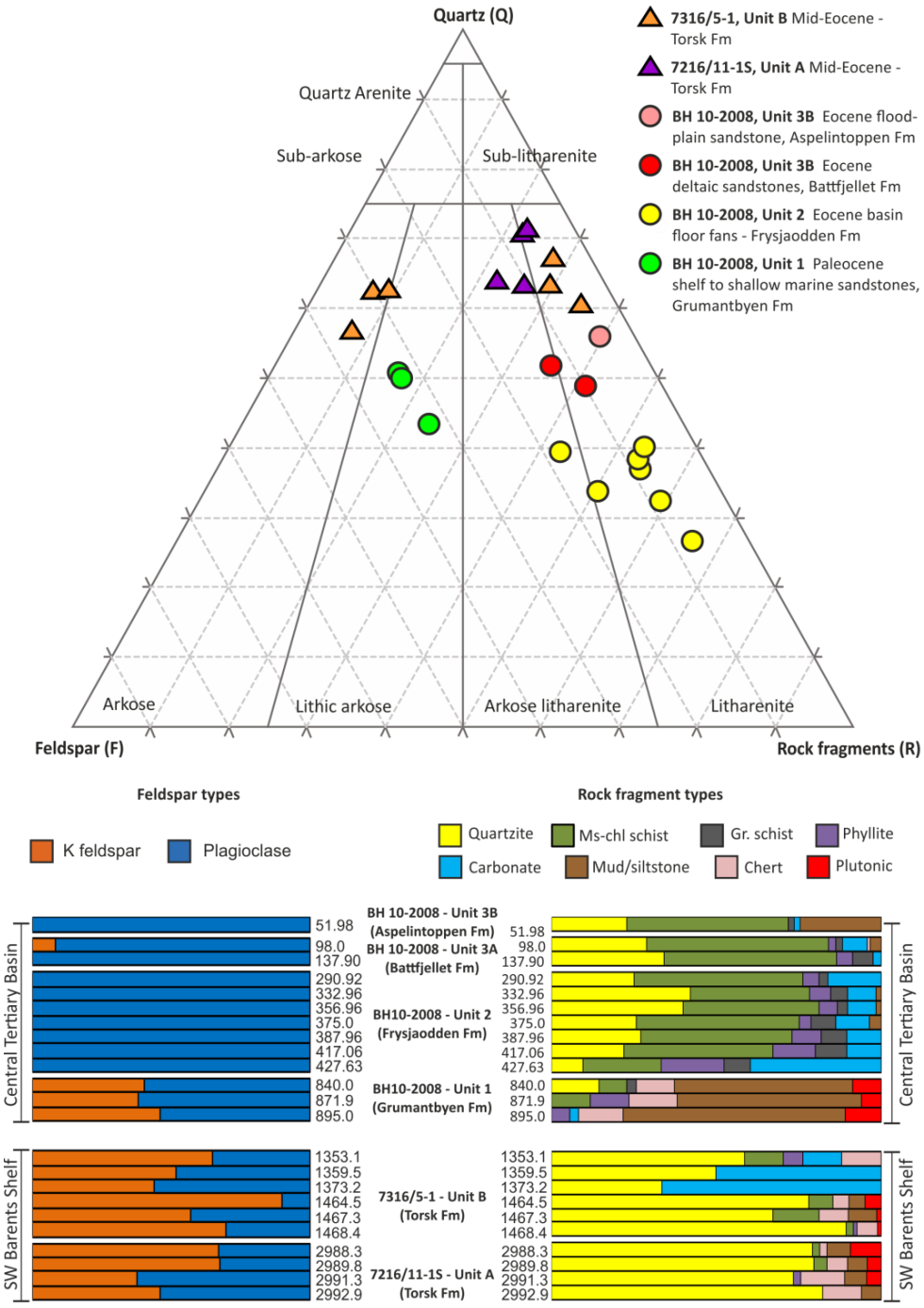

Figure 3. QFR ternary diagram after Folk, Andrews and Lewis [53] determined from petrography on the investigated samples. Feldspar type and rock fragment type proportions are illustrated by the normalised bar charts where Ms-chl schist = Muscovite-chlorite schist and Gr. Schist = Graphitic schist.

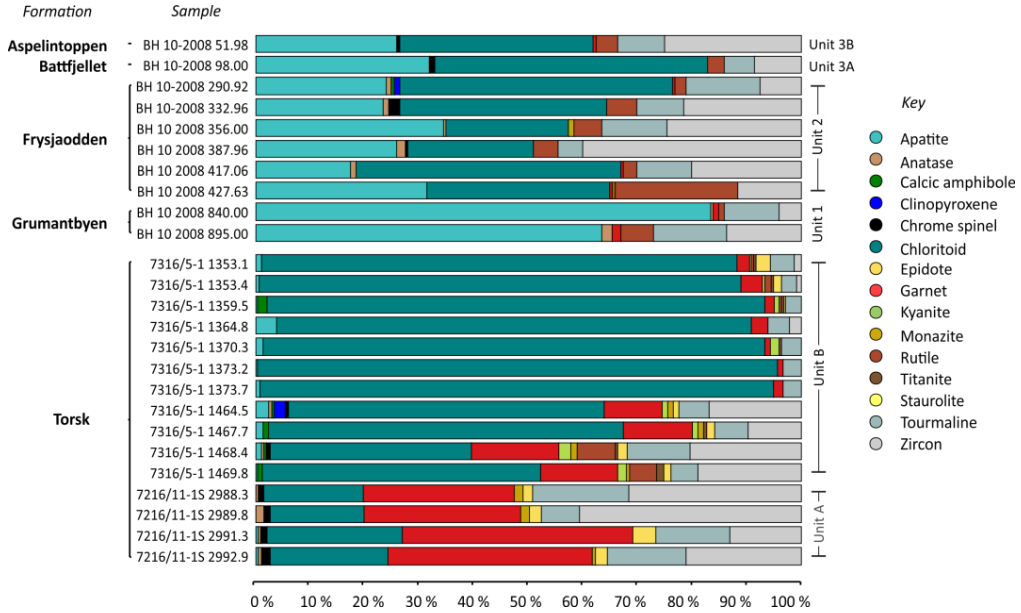

Figure 4. Normalised bar chart showing the non-opaque heavy mineral assemblage of the investigated samples. The order of mineral phases shown in the key appear sequentially from left to right in the bar chart.

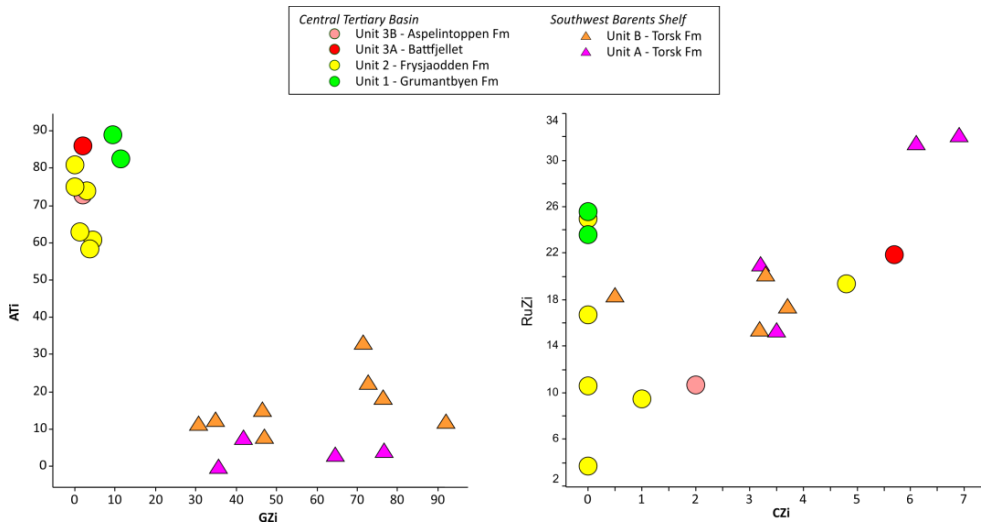

Figure 5. Cross-plots of provenance sensitive heavy mineral indices, after Morton and Hallsworth [54] for the investigated samples. ATi = Apatite-tourmaline index, CZi = chrome spinel-zircon index, GZi = garnet-zircon index, RuZi = rutile-zircon index.

The traditional petrographic and heavy mineral observations are broadly supported by QEMSCAN data (Figure 6). The greater resolution afforded by the SEM analysis has shown that the traditional petrography slightly underestimated plagioclase content and porosity in these samples. The compositional data indicate that the plagioclase is sodic and is classified as albite, and chlorite is Fe-rich and is classified as chamosite. The SEM analysis identified chrome spinel, and by area, a larger proportion of TiO_2 minerals but less apatite than was apparent using the traditional counting.

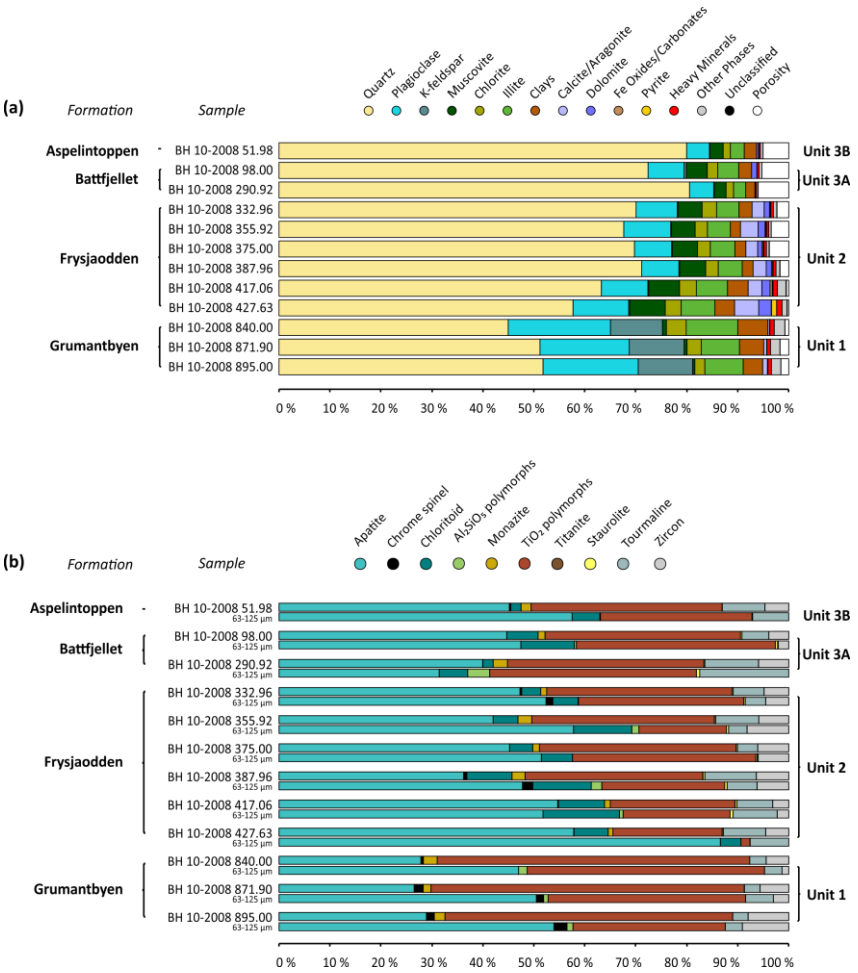

Figure 6. QEMSCAN data (**a**) normalised bar chart showing the modal mineral assemblage, and (**b**) normalised bar charts of the heavy mineral assemblage where for each sample the top bar chart represents the percent area of all grains >5 µm (the resolution of the QEMSCAN images) and the bottom bar chart represents percent area of grains with long axes between 63 and 125 µm.

K-feldspars yield a wide range of Pb isotopic compositions (Figure 7). The majority of the K-feldspars form a spread of radiogenic compositions from a position on the Stacey and Kramers [59] average crustal evolution curve at 300 Ma, to below it. The remainder of the K-feldspars are spread along a broad less radiogenic array located below the average growth curve between 2000 Ma and the radiogenic cluster at 300 Ma.

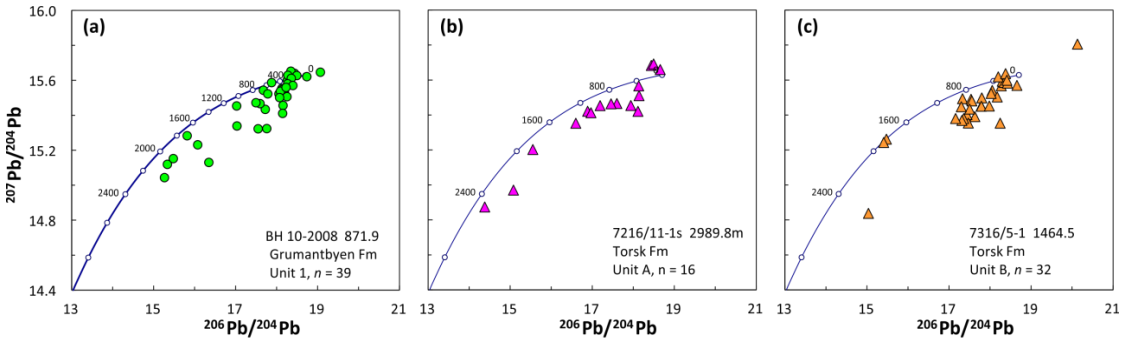

Figure 7. Detrital K feldspar Pb isotopic data for (**a**) Unit 1 of the Grumantbyen Formation from wellbor BH 10-2008, (**b**) Unit A of the Torsk Formation from wellbore 7216/11-1S and (**c**) Unit B of the Torsk Formation from wellbore 7316/5-1. In each plot the curve represents the evolution of average continental crust, taken from Stacey and Kramers [59].

Detrital zircons yield a broad range of U-Pb ages (Figure 8). The most significant age populations are Late Palaeozoic—Early Mesozoic, occurring between 230 Ma and 330 Ma. Other notable populations are centred at *c*. 1870 Ma, 605 Ma, 505 Ma and 180 Ma. Despite the low number of analyses, rutile U-Pb ages mostly coincide with the main 230–330 Ma population recorded in the zircon data. The rutile compositions indicate crystallisation during low temperature conditions and were sourced from metapelitic and metamafic rocks equally (Figure 9). One group of Late Palaeozoic grains is metapelitic and yielded crystallisation temperatures of *c*. 570 °C.

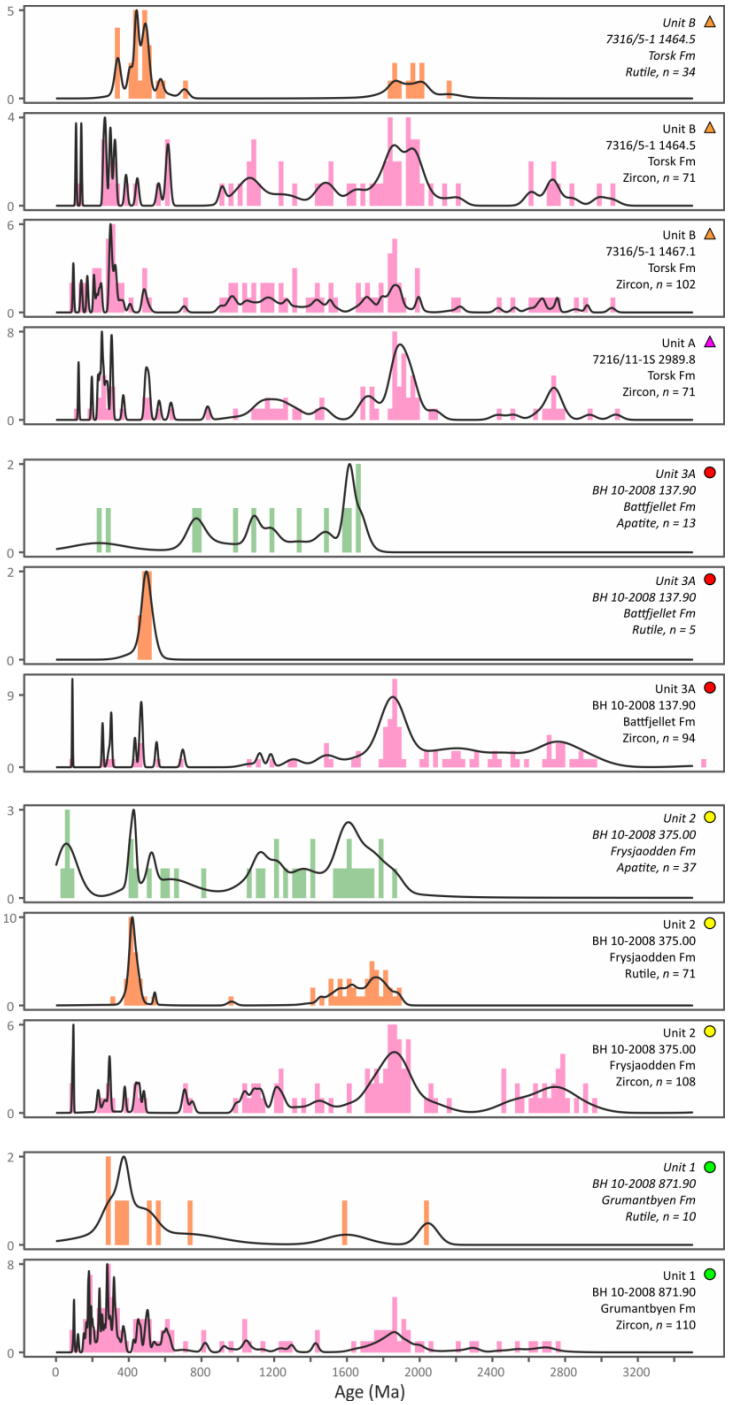

Figure 8. Probability density plots for detrital U-Pb ages determined for zircon (pink), rutile (orange)

and apatite (green). This comparison serves to illustrate how patterns obtained from grains that crystallise under different conditions, and vary with respect to their isotopic closure and susceptibility sedimentary reworking. Generally, zircons record crystallisation from a silicic melts and are readily recycled, rutiles record cooling after metamorphism within pelitic and mafic rocks and are readily recycled, apatites record cooling after crystallisation within melts or during metamorphism in a variety of rock compositions and less likely to be recycled due to their susceptibility to acidic weathering [26]. Data are separated into the different units, symbolised by the coloured circles and triangles as defined on Figure 2. Italicised sample information indicate samples that yielded a low number of reliable analyses and should be interpreted with caution.

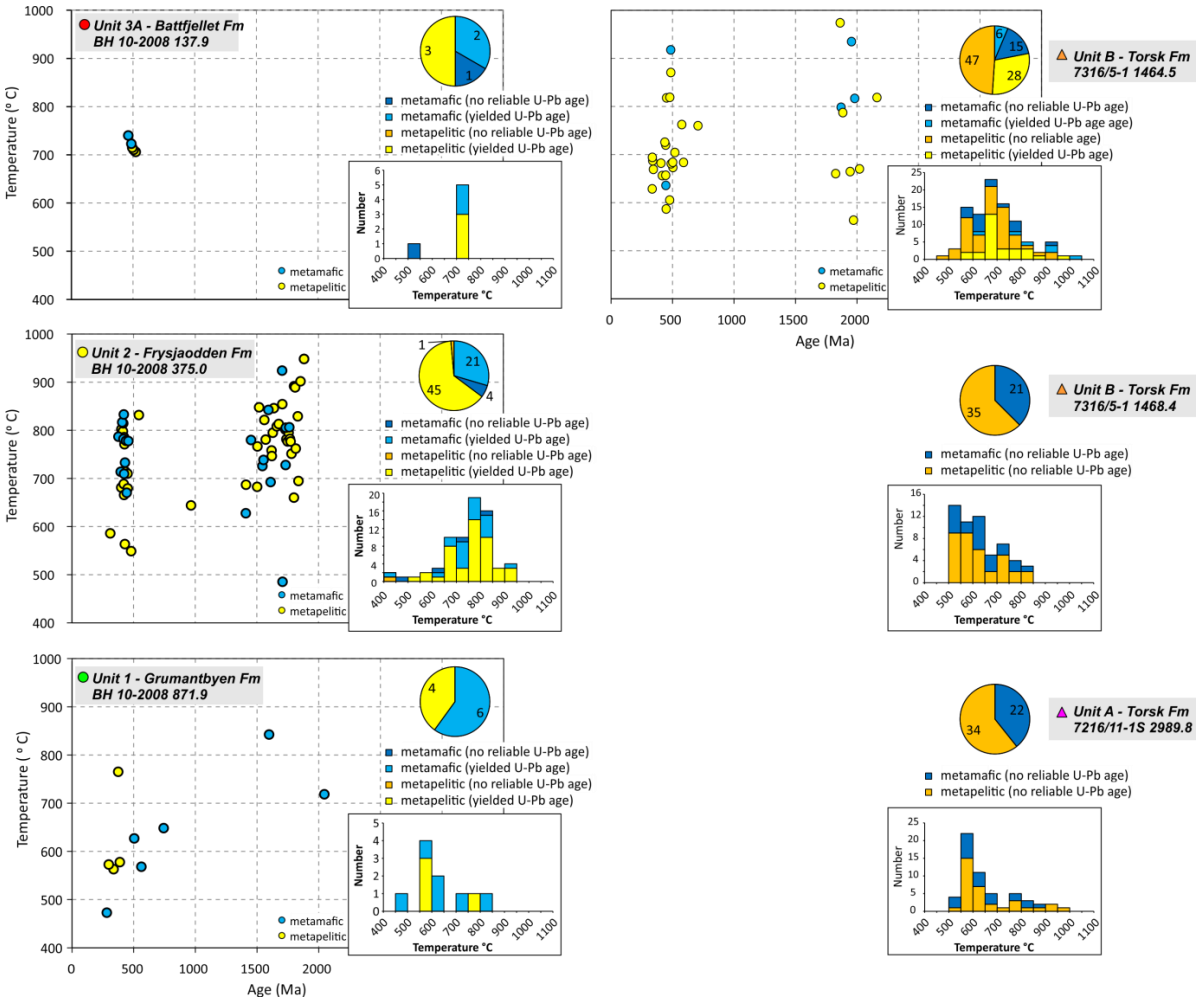

Figure 9. Rutile trace elemental data showing histograms of crystallisation temperature using the Zr in rutile geothermometer of Watson, Wark and Thomas [78] and pie charts of protolith type after Meinhold [77]. The number in the pie chart indicates the number of analyses. The cross plots show the temperature and protolith-type against the calculated U-Pb age for the analyses where reliable U-Pb ages were determined.

4.2. Central Tertiary Basin—Unit 2, Frysjaodden Formation

This unit comprises texturally immature, poorly sorted and moderately to highly compacted sandstones with a predominance of angular grains, that are classified as litharenites (Figure 3). The muscovite and chlorite schist rock fragments are common, as are distinctive graphitic schist and carbonate grains. Plagioclase is the only optically recorded feldspar. The heavy mineral assemblage contains minerals that are generally stable during burial diagenesis, with apatite, chloritoid and zircon most abundant (Figure 4). Provenance sensitive heavy mineral indices record high ATi values and low GZi values in view of the

apatite abundance and lack of garnet. The variable RuZi and CZi values reflect the low variable but generally low abundance of rutile and chrome spinel (Figure 5).

The QEMSCAN data support the petrographic (Figure 6). The plagioclase is sodic and is classified as albite whereas the carbonate is a mixture between calcite and dolomite. The SEM heavy mineral analysis agrees well with the traditional counting method. The lesser proportions of chloritoid identified by QEMSCAN might partly be a function of grain size, as chloritoid is occurs much more commonly in the 63–125 µm grain size, whereas the other heavy mineral species occur more evenly across a wider grain size range (Figure 6).

Detrital zircons yield dominant Palaeoproterozoic and Archaean U-Pb ages, with populations at *c.* 1870 Ma and 2750 Ma (Figure 8). Less commonly occurring Late Mesoproterozoic and Early Palaeozoic populations are also recorded. The two youngest grains yield indistinguishable ages and a 95.1 ± 1.6 Ma weighted mean. Detrital rutiles yield a bimodal U-Pb age distribution, with populations centred on *c.* 1730 Ma and *c.* 420 Ma (Figure 8).

Trace element compositions for the majority of the Palaeoproterozoic grains indicate metapelitic sources and crystallisation temperatures between 750 °C and 850 °C (Figure 9). A broad spread of U-Pb ages resulted from detrital apatites, with populations recorded at *c.* 1610, 1120, 430 and 50 Ma. The youngest population consists of five grains with large uncertainties that result in an imprecise weighted average of 53 ± 27 Ma. The majority of the analysed apatites have very low U contents (<1 ppm), and so did not yield reliable U-Pb ages. Trace element geochemistry indicates that all but one of the analyses without a corresponding U-Pb age plot within the low- and medium-grade metamorphic and metasomatic field of O'Sullivan, Chew, Kenny, Henrichs and Mulligan [80], a field which is very commonly characterized by U-poor apatite. Whilst the grains which yielded ages record a diversity of trace element compositions, the *c.* 53 Ma population plots within the mafic I-type granitoids and mafic igneous rock field, and the *c.* 430 Ma population within the S-type granitoids and high aluminium saturation index felsic I-type granitoid field (Figure 10).

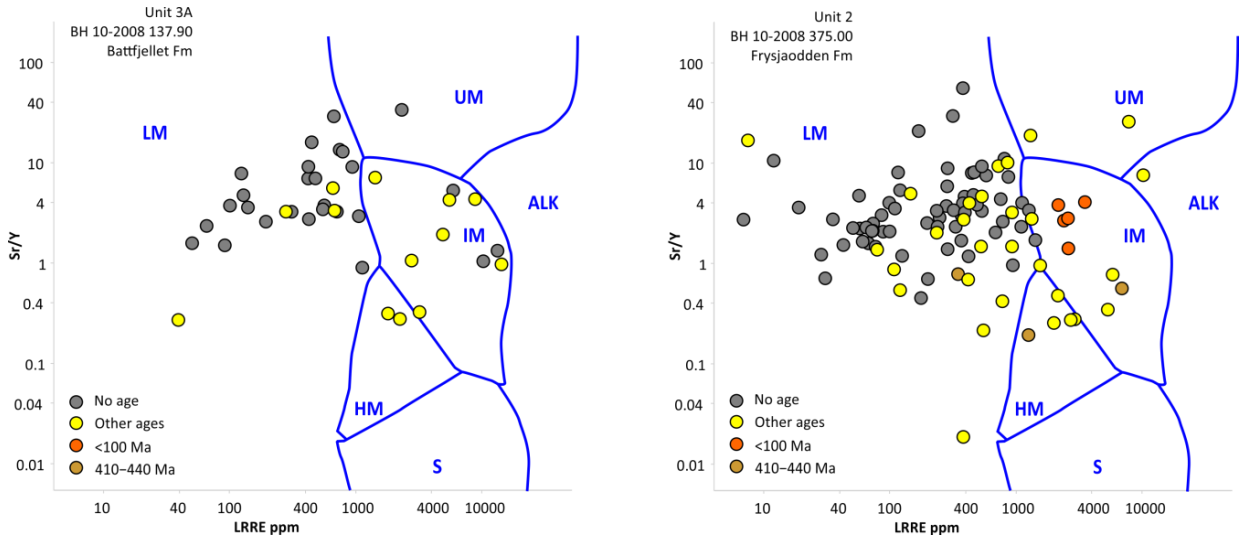

Figure 10. Apatite trace elemental data plotted on the discrimination diagrams from O'Sullivan, Chew, Kenny, Henrichs and Mulligan [80] where ALK = alkali-rich igneous rocks; IM = mafic I-type granitoids and mafic igneous rocks; LM = low- and medium-grade metamorphic and metasomatic; HM = partial-melts/leucosomes/high-grade metamorphic; S = S-type granitoids. Data from grains which also yielded reliable U-Pb age information are indicated.

4.3. Central Tertiary Basin—Units 3A and 3B, Battfjellet and Aspelintoppen Formations

This unit comprises moderately-well sorted and compacted fine-grained sandstones that are texturally immature with a predominance of sub-angular angular grains. The sandstones are classified as litharenites to arkose litharenite (Figure 3) owing to the pre-

ponderance of metamorphic rock fragments and plagioclase feldspar. The heavy mineral assemblage contains minerals that are generally stable during burial diagenesis, but the assemblage is notable for its abundant chloritoid and subordinate chrome spinel (Figure 4). Provenance sensitive heavy mineral indices record high ATi values and low GZi values in view of the apatite abundance and lack of garnet. The variable RuZi and CZi values reflect the relatively low abundance of rutile and chrome spinel compared with zircon (Figure 5).

The quartz-rich nature of the Unit 3 sandstones is also recorded by the QEMSCAN data, which also indicate that plagioclase is sodic and classified as albite (Figure 6). By area, SEM analysis indicates that TiO_2 polymorphs are more important than rutile recorded by the traditional heavy mineral counting method. However, this may be due to the SEM method being unable to separate TiO_2 polymorphs.

Detrital zircons have mostly Palaeoproterozoic and Archaean ages, with one dominant population at *c*. 1850 Ma with a subordinate population at *c*. 2705 Ma (Figure 8). Younger grains are uncommon, a single grain with a 90.4 ± 4.2 Ma calculated age being the youngest recorded. Just six rutile grains were analysed, which are spread equally between metamafic and metapelitic varieties and record crystallisation temperatures between 700 and 750 °C. U-Pb ages for these grains form a *c*. 490 Ma population (Figure 9). Few analysed apatite grains yielded precise U-Pb ages; those that did yielded a range of ages (Figure 8). Trace element geochemistry indicates that the majority of analysed grains without a corresponding U-Pb age plot within the low- and medium-grade metamorphic and metasomatic field of O'Sullivan, Chew, Kenny, Henrichs and Mulligan [80], and also have low uranium contents. The low numbers of reliable rutile and apatite U-Pb ages obtained from this sample means in isolation, they should be interpreted with caution.

4.4. Southwest Barents Shelf—Unit A, Torsk Formation

The wellbore 7216/11-1S sandstones from Unit A are weakly-compacted and cemented, fine-grained, and poorly- to moderately-sorted. Grains are generally sub-rounded and comprise predominantly quartz with subordinate feldspar, which is equally distributed between plagioclase and alkali feldspar varieties. The sands are classified as arkose litharenite and litharenite, with equal proportions of alkali and plagioclase feldspar, and abundant quartzite and chert rock fragments (Figure 3). The heavy mineral assemblage is diverse containing garnet, chloritoid, chrome spinel and staurolite, in addition to the stable minerals rutile, tourmaline and zircon (Figure 4), which yield low ATi and high CZi and GZi values (Figure 5).

K-feldspars yield a range of Pb isotopic compositions (Figure 7), between a position on the Stacey and Kramers [59] average crustal evolution curve at 300 Ma to one below it with $^{206}Pb/^{204}Pb$ values of *c*. 15, the latter consistent with Palaeoproterozoic and Archaean sources. Detrital zircons from sample 7216/11-1S 2989.8 yield a broad range of U-Pb ages (Figure 8). Most significant age populations occur in the Palaeoproterozoic between 1800 Ma and 2000 Ma, most notably with a *c*. 1870 Ma group, and in the Late Palaeozoic between 250 Ma and 350 Ma. Rutile trace element compositions from this sample indicate that the majority of grains crystallised within metapelitic rocks and crystallised with metamorphic temperatures of 550–650 °C (Figure 9).

4.5. Southwest Barents Shelf—Unit B, Torsk Formation

Samples from Unit B come from wellbore 7316/5-1, and are weakly cemented or are uncemented. The samples are moderately- to poorly-sorted with grains sizes between coarse silt to very fine sand and are classified as arkoses, with approximately equal proportions of alkali and plagioclase feldspar (Figure 3). Rock fragments contain silica-rich metamorphic and in the shallower samples carbonaceous varieties are important. The heavy mineral assemblage is very distinct and is dominated by chloritoid, dramatically so for the shallower samples of depths between 1373.7 and 1353.1 m (Figure 4), which also and contain very low quantities of rutile, tourmaline and zircon. Some samples also contain small quantities of unstable grains including calcic amphibole and clinopyroxene.

Chrome spinel is a minor component of the assemblage and apatite notably occurs in low abundance (Figure 4). Provenance sensitive indices correspondingly yield moderate GZi and RuZi values and low ATi and CZi values (Figure 5). Provenance sensitive indices result in high GZi values and low to moderate ATi values (Figure 5), but the scarcity of zircon, rutile and chrome spinel recorded in some samples meant that CZi and RuZi indices could not be determined for all samples.

K-feldspar Pb isotopic compositions are similar to Unit A of the Torsk Formation and form an array between a 300 Ma position on the Stacey and Kramers [59] average continental crustal evolution curve to one below it with $^{206}Pb/^{204}Pb$ values of *c.* 17.5 (Figure 7). In addition, there are a few grains with less radiogenic compositions and lower $^{206}Pb/^{204}Pb$, consistent with Archaean or Palaeoproterozoic sources.

For sample 7316/5-1 1464.5, U-Pb rutile age data were concurrently collected with trace element geochemistry. The ages are predominantly Late Palaeozoic and subordinately Palaeoproterozoic (Figure 8). Rutile and zircon U-Pb ages populations overlap, although the rutile analyses yield a greater proportion of *c.* 420 and 480 Ma grains than are evident in the zircon data. The rutiles grains that yielded reliable ages mostly crystallised under temperatures <700 °C within metapelitic rocks during the Late Palaeozoic (Figure 9), however a much greater number of grains yield higher temperature values than is evident from Unit A of the Torsk Formation.

5. Provenance Interpretations and Discussion

5.1. Provenance Variation Recorded within the Central Tertiary Basin

The new data from wellbore BH 10-2008 are closely aligned with previous provenance interpretations from the Paleogene strata of the Central Tertiary Basin on Spitsbergen, e.g., [16]. The BH 10-2008 data document the influx and subsequent dominance of a new sediment source terrain between deposition of the Unit 1 and Unit 2 sandstones of the Paleocene Grumantbyen and Eocene Frysjaodden formations, respectively.

In view of the fact that around one quarter of the sand grains from Unit 1 sandstones of the Grumantbyen Formation are feldspar (Figures 3 and 6), it follows that a significant portion of the Paleocene sand was sourced directly from crystalline granitoid rocks. The occurrence of Palaeoproterozoic and Palaeozoic zircon populations overlap in age with those obtained from crystalline basement and granites from northeast Svalbard, e.g., [81,82]. The K-feldspar Pb compositions suggest the greatest contribution was from Caledonian granitoids.

The existence of chert and shale rock fragments but the absence of metamorphic rock fragments indicates that an additional sediment source may have been recycled from a sedimentary succession unaffected by tectonic and metamorphic events. The high apatite content and ATi values from the heavy mineral assemblage and presence of minor proportions of chrome spinel, coupled with zircon and rutile grains with Late Palaeozoic–Early Mesozoic age would suggest recycling of the Triassic succession east of the Central Tertiary Basin. This interpretation fits with substantial erosion of the Triassic east of Svalbard since the Cretaceous, as suggested by Gilmullina, Klausen, Doré, Sirevaag, Suslova and Eide [34] and with the synopsis of regional detrital zircon patterns shown by the multi-dimension scaling (MDS) plot on Figure 11.

On the MDS plot, sample BH 10-2008 871.9 is located along a mixing line between easterly sourced Triassic strata and strata with zircon age patterns that are provenance insensitive [83]; a scenario that is also consistent with sand being eroded from crystalline basement mixing with material presumably recycled from the easterly-sourced Triassic. The provenance and sedimentological data thus indicate the presence of an exhumed terrain lying broadly east and north of the Central Tertiary Basin (Figure 12), possibly resulting from forebulge uplift associated with the first stages of Eurekan deformation [10].

The provenance signatures of the Unit 2 sandstones of the Eocene Frysjaodden Formation contrast markedly with those from Unit 1 and indicate differing provenance. The generally angular grains are consistent with short sediment transport distances, and the

dominance of albitic plagioclase, schist rock fragments and the lack of K-feldspar indicate erosion from high greenschist- or low amphibolite-facies grade metasedimentary units. The distinctive occurrence of chloritoid and abundance of apatite with low U and low LREE contents supports a low-grade metamorphic origin for these sand-grade deposits.

Recycled zircons would be expected from such low-grade metasedimentary units. The dominance of Archaean and Palaeoproterozoic grains between 1800 Ma and 2800 Ma recorded from sample BH 10-2008 375.0 indicate that these were originally sourced from the Greenland craton. The addition of a smaller number of grains with Mesoproterozoic ages suggest that Late Neoproterozoic metasedimentary units were also eroded. This is documented by the MDS analysis as the sample plots along a mixing line between Greenland and regions with provenance insensitive signatures (Figure 11). Detrital rutile age peaks at 1730 Ma and 420 Ma might be taken as evidence that metasedimentary sources had experienced orogeny and metamorphism at those times. However, given the duplication of these age peaks in the apatite data, and the fact that most of the analysed apatite was metamorphic did not yield ages (Figure 10), it is perhaps more likely that the dated rutile and apatite are also recycled detrital grains and that the deformation event affecting the metasedimentary units occurred after the Caledonian Orogeny. Greenschist- to low amphibolite-facies metasedimentary rocks are recorded from the North Greenland fold belt which formed during Late Devonian Ellesmerian deformation [84]. These metamorphic rocks contain abundant chloritoid [85], which could explain its high abundance in the heavy mineral assemblage. The five youngest apatite grains with mafic igneous trace element compositions and a 59 $\pm$ 24 Ma weighted average age overlap with volcanic units exposed at Kap Washington in North Greenland [86], and may indicate a possible source for these grains.

The high degrees of Eocene exhumation recorded from western Spitsbergen [3] and the presence of chloritoid recorded from metamorphic rocks on west Spitsbergen and Prins Karls Forland [87,88], indicates that the source region may be more proximal than north Greenland. However, zircon patterns from these and other similar Neoproterozoic and Early Palaeozoic metasedimentary units contained within the Southwest Basement Province [89] contain abundant grains with ages between 900 and 1700 Ma, e.g., [90], ages are much less commonly occurring in the Unit 2 sandstone sample. The recycled zircon pattern in the Eocene sandstones require an additional source, thus while this west Svalbard proximal source may have contributed to the sediment budget, it was likely a minor component. More northerly portions of the basin [30] might have a contribution from the Northwestern Basement Province, which records similar zircon patterns to the Southwest Province units [91], but because it is variably migmatised and intruded by granitoids associated with Caledonian deformation and metamorphism, any source from this province would be expected to contain Silurian grains.

Figure 11. Multi-dimensional scaling (MDS) plot of detrital zircons from samples collected from the Barents Shelf region. Data are simplified to show the inferred sediment source and/or location of the successions. Plot constructed following Vermeesch [92] and Vermeesch et al. [93] and is constructed from data obtained from 186 samples [13,16,27,45–48,90,94–111] from the Barents Shelf and adjacent regions. The goodness of fit, describing how well the data can be represented on a 2D plane, is indicated by the stress value. Stress values of this magnitude are considered fair [112]. Data from the Central Tertiary Basin and the Torsk Formation are highlighted by points with bold outlines, and those obtained in this study are labelled. The grey dashed ellipse represents samples with dominant Mesoproterozoic-Late Neoproterozoic populations, because of which their recycled nature have been shown to have reduced provenance significance in this region of the Arctic [83] and the grey arrowed line represents a mixture between north Greenland and Barents Shelf sources.

In combination, the provenance indicators point to a sediment source region located within the Eurekan deformation zone, likely in north Greenland. The eroded units include the Proterozoic platform and Palaeozoic Franklinian Basin units metamorphosed during Late Devonian Ellesmerian tectonism. The low number of zircons with ages between

235 Ma and 360 Ma further suggest that Triassic deposits within the Eurekan deformation zone, such as those exposed in north Greenland [113], were either not eroded during the Eocene or that the Uralian signature that characterizes the Triassic on the Barents Shelf was less prominent in north Greenland [114]. As expected, given the genetic link between the basin floor fans and the overlying deltaic succession, there is no appreciable difference between the provenance of Unit 2 sandstones of the Frysjaodden Formation and Unit 3 sandstones of the Battfjellet and Aspelintoppen formation. However, Unit 3B sandstones contain a minor component of K-feldspar, which may signify inversion of the basin and reworking of Unit 1 sandstones as the Eurekan deformation progressed.

5.2. Linking the Torsk Formation Sands with Paleogene Sandstones on Spitsbergen

The sediment provenance indicators from Units A and B from the Torsk Formation show a mix of features that are characteristic of east Barents Shelf-derived Unit 1 sandstones and Eurekan-derived Unit 2/3 sandstones of the Central Tertiary Basin. For instance, the abundance and Pb isotopic composition of K-feldspar is a distinctive characteristic of the easterly sourced sandstones of Unit 1, whereas the dominance of chloritoid in the heavy mineral assemblage is a distinctive characteristic of sandstones of Units 2 and 3 from the Central Tertiary Basin. Differences in the heavy mineral assemblage likely highlights the impact of weathering and storage during transport and subsequent burial diagenesis; the lack of apatite from the Torsk Formation sandstones highlights prolonged weathering and the greater abundance of chloritoid, garnet and staurolite indicate much less severe burial dissolution effects compared with the Central Tertiary Basin sandstones. The apparent mixed provenance signal is replicated in the rutile and zircon U-Pb data, and is clearly illustrated in Figure 11 where the zircon ages where the Torsk samples plot along a mixing line between the two Central Basin sand types.

If the provenance signatures indicate a mixture of the Eurekan and eastern Barents Shelf source terrains, it remains highly uncertain from where within these two regions the Torsk sediments were derived and where they got mixed. Clues come from the spread of U-Pb zircon ages in the 225 Ma to 450 Ma interval. The majority of the zircons from the Torsk Formation sandstones that fall within the range are 250 Ma to 330 Ma. However, the Unit 1 sandstones have an expanded range of ages, including minor 235 Ma and 425 Ma populations. These signals are consistent with the Torsk Formation sandstones being in part recycled from Triassic sediments that were deposited on southern parts of the Barents Shelf, whereas the Unit 1 sandstones were being in part recycled from Triassic sediments that were deposited on northern parts of the Barents Shelf. This is because the Triassic deposited in the south contain less voluminous *c*. 235 Ma and 420 Ma populations than those deposited in the north, owing to their differing provenance [47]. Although the Triassic succession of the Barents Shelf also contains chloritoid, it is not sufficiently abundant to be detected in such high quantities as is recorded from the Torsk Formation sandstones [47].

Some workers infer that structural highs, such as the Loppa and Stappen High on the southwestern margin of the Barents Shelf, provided sediment to the Torsk Formation [19,20]. Sources from the Stappen High would likely have eroded Cretaceous strata that had a northerly source [43,44]. As such, it is possible that the Cretaceous strata share many of the mixed provenance signals recorded from the Torsk Formation. Although comparable data from Lower Cretaceous strata are not available, it may in any case be difficult from the provenance data to unravel local high versus distal shelf contributions to the Torsk Formation sandstones. As the northerly sourced Cretaceous succession was not deposited on the Loppa High, Jurassic and Triassic strata would have been reworked from this high. On the basis of the zircon spectra at least, it is unlikely that this was an important sediment source because the Jurassic and Latest Triassic contain predominantly Mesoproterozoic grains [45,46], and these are not very abundant in the Torsk Formation samples investigated here.

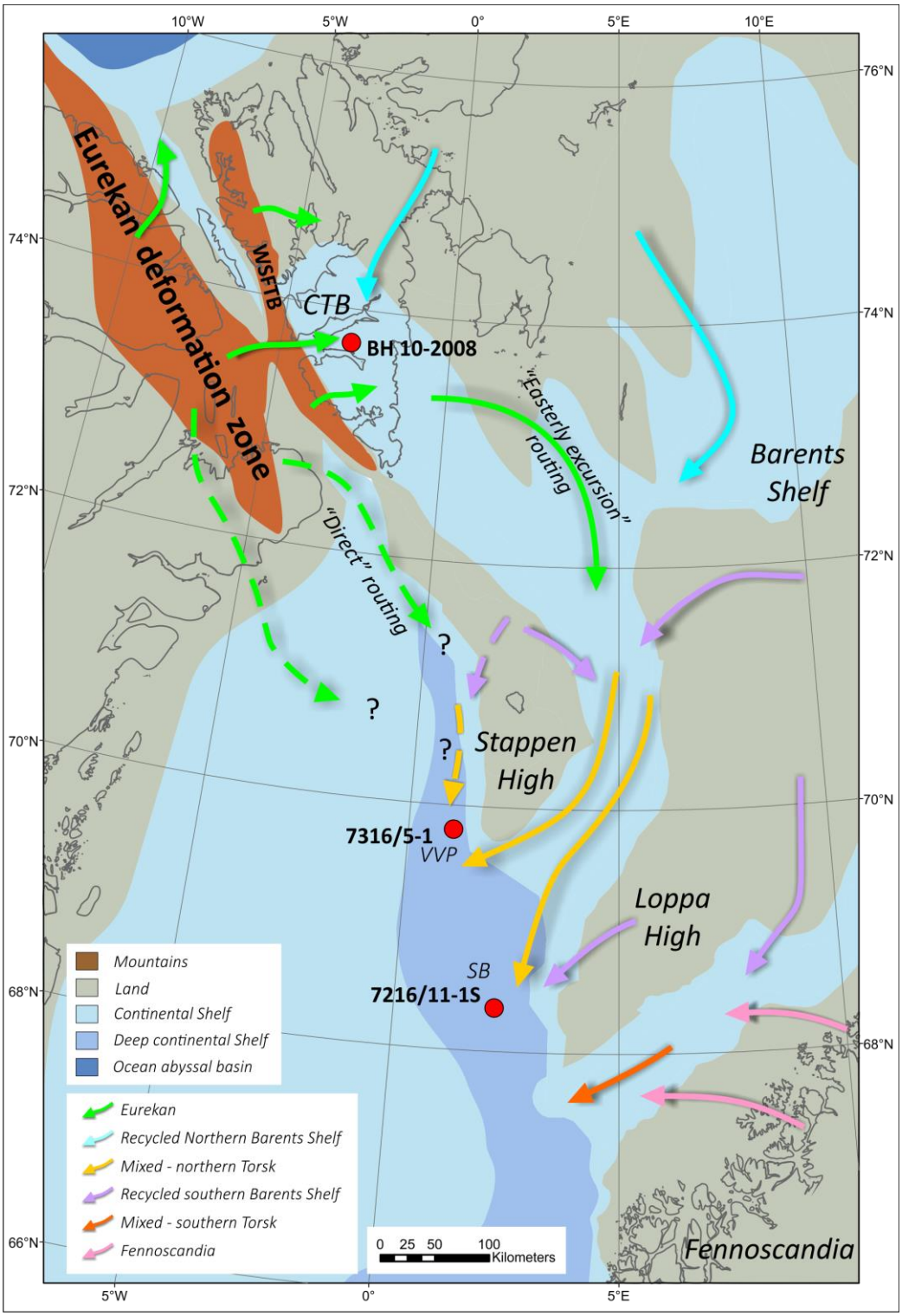

Figure 12. Schematic Eocene palaeogeography adapted from Blakey [4], Smelror, Petrov, Larssen and Werner [5], Helland-Hansen and Grundvåg [9] and Lasabuda, Laberg, Knutsen and Høgseth [19] showing possible Eocene sediment routing on the western Barents Shelf, based on a 50 Ma GPlates reconstruction [115]. Direct and less certain routing from the terrains exhumed during Eurekan deformation are shown as dashed arrows, whereas more certain Eurekan-derived sediment pathways are shown as solid lines. CTB = Central Tertiary Basin, SB = Sørvesstnaget Basin, VVP = Vesybakken Volcanic Province and WSFTB = West Spitsbergen fold-and-thrust Belt.

The provenance data presented here is consistent with a fill and spill model for the Central Tertiary Basin [9] is consistent with the provenance data (Figure 12). More direct routing from the exhumed Eurekan terrains would need to bypass the wide northeast Greenland Shelf. The thin Eocene sedimentary succession there [116] could indicate significant bypass, however, any sediment pathway would need to circumnavigate depocentres and localised regions of uplift, such as the Stappen and Loppa highs, associated with transtensional pull apart basins generated by rotation of Greenland relative to Svalbard [25,117]. Although possible, this more direct routing (dashed green arrows on Figure 12) would seem less likely than one which took an easterly 'excursion' (solid green arrows on Figure 12) across the Barents Shelf. Southern portions of the Torsk Formation possibly also sourced sediment from Fennoscandia (Figure 12).

The interpretations outlined here result from a framework of provenance data. The model may be tested and refined with further analyses. In particular there is a great need for an increased sample set from the Battfjellet and Aspelintoppen formations from the Central Tertiary Basin, as these units may more closely resemble the sediment composition of distributed farther south across the Barents Shelf. Larger samples than 40 g would ensure greater heavy mineral yields, increasing the likelihood of statistically useful datasets for all provenance techniques. In this study, low apatite and rutile yields have been encountered. In addition, study of Eocene samples from wells located west of the Hammerfest Basin and from the northeast Greenland Shelf could assess Fennoscandian contributions and test direct pathway to the southwest margin of the Barents Shelf for the Eurekan-derived sediment.

6. Conclusions

The Eocene topography that formed within the Eurekan deformation zone of north Greenland and the West Spitsbergen Fold-and-Thrust Belt was eroded and the resultant sediment was transported to the Spitsbergen Central Tertiary Basin. This Eurekan-derived sediment has distinctive provenance indicators, characterised by albitic plagioclase feldspar, metasedimentary schist rock fragments, a heavy mineral assemblage with abundant chloritoid, metamorphic apatite with low REE contents, metapelitic rutile with Silurian U-Pb ages and zircons with predominantly Archaean and Palaeoproterozoic U-Pb age populations. All of these indicators are consistent with the eroded strata being originally sourced from Greenland and being metamorphosed during Late Devonian Ellesmerian tectonism. This is consistent with previous field and sedimentological observations.

During the initial phase of Eurekan deformation in the Paleocene, a separate sediment source delivered material to the Spitsbergen Central Tertiary Basin. This material is characterised by the presence of K-feldspar with radiogenic Pb isotopic compositions, chrome spinel in the heavy mineral assemblage, and detrital zircons and rutiles with prominent Palaeoproterozoic and Late Palaeozoic—Early Mesozoic U-Pb age populations together suggest the Paleocene sediments were sourced directly from Palaeoproterozoic crystalline basement to the north and reworked from Triassic strata from the eastern parts of the Barents Shelf, the latter possibly being an expression of a forebulge associated with Eurekan uplift.

The Eocene Torsk Formation was deposited within transtensional pull-apart basins on the southwest Barents Shelf margin and contain provenance signatures characteristic of both Eurekan and eastern Barents Shelf source terrains. The dominance of chloritoid and garnet in the heavy mineral record, coupled with mixed detrital zircon signatures indicates that the Torsk Formation sandstones were sourced from either the Eurekan deformation zone or the Fennoscandian Shield. As chloritoid is not a dominant feature of sediment sourced from Fennoscandia a fill and spill model for the Central Tertiary Basin is proposed, thus offering an explanation for the mixed signals documented in the Torsk Formation. During the Eocene, Eurekan-derived sediment was first routed east and eventually filled the foreland basin, then turned to the south shedding sediment across the Barents Shelf where the Eurekan sediments became mixed with locally reworked Mesozoic successions. Through this study that utilises multiple and complementary provenance techniques,

new light is shed on regional source-to-sink patterns of the early Cenozoic succession of the western Barents Shelf region, highlighting the importance of tectonically-induced topography on sediment fairways.

Supplementary Materials: The following supporting information can be downloaded at: https://www.mdpi.com/article/10.3390/geosciences13030091/s1, Table S1: petrography; Table S2: heavy mineral analysis; Table S3: QEMSCAN data; Table S4: K-feldspar Pb isotopic data; Table S5: apatite U-Pb geochronology and trace element data; Table S6: rutile U-Pb geochronology and trace element data; Table S7: zircon U-Pb geochronology.

Author Contributions: Conceptualization and methodology, M.J.F. and E.J.F.; validation, D.M.C., D.F., A.B., E.B. and M.J.W.; formal analysis, M.J.F.; investigation, A.C.M., D.F., J.O. and T.R.R.; writing—original draft preparation, M.J.F.; writing—review and editing, E.J.F., D.M.C., A.C.M., T.R.R. and E.B.; visualization, M.J.F.; supervision, M.J.F.; project administration, M.J.F. All authors have read and agreed to the published version of the manuscript.

Funding: This research received no external funding.

Acknowledgments: This research was carried out as part of CASP's Barents Shelf Provenance Project. Our sponsors' financial support is gratefully acknowledged. This is NORDSIMs publication number 728. This paper has benefitted from the careful and constructive revision recommended by three anonymous journal reviewers.

Conflicts of Interest: The authors declare no conflict of interest.

References

1. Piepjohn, K.; Von Gosen, W.; Tessensohn, F. The Eurekan deformation in the Arctic: An outline. *J. Geol. Soc.* **2016**, *173*, 1007–1024. [CrossRef]
2. Vamvaka, A.; Pross, J.; Monien, P.; Piepjohn, K.; Estrada, S.; Lisker, F.; Spiegel, C. Exhuming the Top End of North America: Episodic Evolution of the Eurekan Belt and Its Potential Relationships to North Atlantic Plate Tectonics and Arctic Climate Change. *Tectonics* **2019**, *38*, 4207–4228. [CrossRef]
3. Dörr, N.; Lisker, F.; Clift, P.D.; Carter, A.; Gee, D.G.; Tebenkov, A.M.; Spiegel, C. Late Mesozoic-Cenozoic exhumation history of northern Svalbard and its regional significance: Constraints from apatite fission track analysis. *Tectonophysics* **2012**, *514–517*, 81–92. [CrossRef]
4. Blakey, R. Paleotectonic and paleogeographic history of the Arctic region. *Atl. Geosci.* **2021**, *57*, 007–039. [CrossRef]
5. Smelror, M.; Petrov, O.V.; Larssen, G.B.; Werner, S.C. *Atlas: Geological History of the Barents Sea*; Geological Survey of Norway: Trondheim, Norway, 2009; p. 134.
6. Steel, R.J.; Dalland, A.; Kalgraff, K.; Larsen, V. (Eds.) *The Central Tertiary Basin of Spitsbergen: Sedimentary Development of a Sheared-Margin Basin*; Canadian Society of Petroleum Geologists: Calgary, AB, Canada, 1981; Volume 7, pp. 647–664.
7. Steel, R.; Gjelberg, J.; Helland-Hansen, W.; Kleinspehn, K.; Nøttvedt, A.; Rye-Larsen, M. The Tertiary Strike-Slip Basins and Orogenic Belt of Spitsbergen. *Strike-Slip Deform. Basin Form. Sediment.* **1985**, *37*, 339–359. [CrossRef]
8. Müller, R.D.; Spielhagen, R.F. Evolution of the Central Tertiary Basin of Spitsbergen: Towards a synthesis of sediment and plate tectonic history. *Palaeogeogr. Palaeoclimatol. Palaeoecol.* **1990**, *80*, 153–172. [CrossRef]
9. Helland-Hansen, W.; Grundvåg, S.-A. The Svalbard Eocene-Oligocene (?) Central Basin succession: Sedimentation patterns and controls. *Basin Res.* **2021**, *33*, 729–753. [CrossRef]
10. Bruhn, R.; Steel, R. High-resolution sequence stratigraphy of a clastic foredeep succession (Paleocene, Spitsbergen): An example of peripheral-bulge-controlled depositional architecture. *J. Sediment Res.* **2003**, *73*, 745–755. [CrossRef]
11. Helland-Hansen, W. Sedimentation in Paleogene foreland basin, Spitsbergen. *Assoc. Pet. Geol. Bull.* **1990**, *74*, 260–272. [CrossRef]
12. Lüthje, C.J.; Nichols, G.; Jerred, R. Sedimentary facies and reconstruction of a transgressive coastal plain with coal formation, Paleocene, Spitsbergen, Arctic Norway. *Norw. J. Geol.* **2020**, *100*, 202010. [CrossRef]
13. Elling, F.J.; Spiegel, C.; Estrada, S.; Davis, D.W.; Reinhardt, L.; Henjes-Kunst, F.; Allroggen, N.; Dohrmann, R.; Piepjohn, K.; Lisker, F. Origin of Bentonites and Detrital Zircons of the Paleocene Basilika Formation, Svalbard. *Front. Earth Sci.* **2016**, *4*, 73. [CrossRef]
14. Grundvåg, S.A.; Johannessen, E.P.; Helland-Hansen, W.; Plink-Björklund, P. Depositional architecture and evolution of progradationally stacked lobe complexes in the Eocene Central Basin of Spitsbergen. *Sedimentology* **2014**, *61*, 535–569. [CrossRef]
15. Petter, A.L.; Steel, R.J. Hyperpycnal flow variability and slope organization on an Eocene shelf margin, Central Basin, Spitsbergen. *AAPG Bull.* **2006**, *90*, 1451–1472. [CrossRef]
16. Petersen, T.G.; Thomsen, T.B.; Olaussen, S.; Stemmerik, L. Provenance shifts in an evolving Eurekan foreland basin: The Tertiary Central Basin, Spitsbergen. *J. Geol. Soc.* **2016**, *173*, 634. [CrossRef]

17. Helland-Hansen, W. Facies and stacking patterns of shelf-deltas within the Palaeogene Battfjellet Formation, Nordenskiöld Land, Svalbard: Implications for subsurface reservoir prediction. *Sedimentology* **2010**, *57*, 190–208. [CrossRef]
18. Safronova, P.A.; Henriksen, S.; Andreassen, K.; Laberg, J.S.; Vorren, T.O. Evolution of shelf-margin clinoforms and deep-water fans during the middle Eocene in the Sorvestsnaget Basin, southwest Barents Sea. *AAPG Bull.* **2014**, *98*, 515–544. [CrossRef]
19. Lasabuda, A.; Laberg, J.S.; Knutsen, S.-M.; Høgseth, G. Early to middle Cenozoic paleoenvironment and erosion estimates of the southwestern Barents Sea: Insights from a regional mass-balance approach. *Mar. Pet. Geol.* **2018**, *96*, 501–521. [CrossRef]
20. Ryseth, A.; Augustson, J.H.; Charnock, M.; Haugerud, O.; Knutsen, S.M.; Midbøe, P.S.; Opsal, J.G.; Sundsbø, G. Cenozoic stratigraphy and evolution of the Sørvestsnaget Basin, southwestern Barents Sea. *Nor. Geol. Tidsskr.* **2003**, *83*, 107–130.
21. Bergh, S.G.; Grogan, P. Tertiary structure of the Sørkapp-Hornsund Region, South Spitsbergen, and implications for the offshore southern extension of the fold-thrust Belt. *Nor. Geol. Tidsskr.* **2003**, *83*, 43–60.
22. Riis, F. Quantification of Cenozoic vertical movements of Scandinavia by correlation of morphological surfaces with offshore data. *Glob. Planet Chang.* **1996**, *12*, 331–357. [CrossRef]
23. Faleide, J.I.; Myhre, A.M.; Eldholm, O. Early Tertiary volcanism at the western Barents Sea margin. *Geol. Soc. Lond. Spec. Publ.* **1988**, *39*, 135–146. [CrossRef]
24. Kristensen, T.B.; Rotevatn, A.; Marvik, M.; Henstra, G.A.; Gawthorpe, R.L.; Ravnås, R. Structural evolution of sheared margin basins: The role of strain partitioning. Sørvestsnaget Basin, Norwegian Barents Sea. *Basin Res.* **2018**, *30*, 279–301. [CrossRef]
25. Libak, A.; Eide, C.H.; Mjelde, R.; Keers, H.; Flüh, E.R. From pull-apart basins to ultraslow spreading: Results from the western Barents Sea Margin. *Tectonophysics* **2012**, *514–517*, 44–61. [CrossRef]
26. Chew, D.; O'Sullivan, G.; Caracciolo, L.; Mark, C.; Tyrrell, S. Sourcing the sand: Accessory mineral fertility, analytical and other biases in detrital U-Pb provenance analysis. *Earth-Sci. Rev.* **2020**, *202*, 103093. [CrossRef]
27. Flowerdew, M.J.; Fleming, E.J.; Morton, A.C.; Frei, D.; Chew, D.M.; Daly, J.S. Assessing mineral fertility and bias in sedimentary provenance studies: Examples from the Barents Shelf. *Geol. Soc. Lond. Spec. Publ.* **2020**, *484*, 255. [CrossRef]
28. Harland, W.B.; Kelly Simon, R.A.; Geddes, I.; Doubleday Paul, A. Chapter 4 The Central Basin. *Geol. Soc. Lond. Mem.* **1997**, *17*, 47–74. [CrossRef]
29. Dörr, N.; Lisker, F.; Jochmann, M.; Rainer, T.; Schlegel, A.; Schubert, K.; Spiegel, C. Subsidence, rapid inversion, and slow erosion of the Central Tertiary Basin of Svalbard: Evidence from the thermal evolution and basin modeling. In *Circum-Arctic Structural Events: Tectonic Evolution of the Arctic Margins and Trans-Arctic Links with Adjacent Orogens*; Geological Society of America: Boulder, CO, USA, 2019; Volume 541.
30. Jochmann, M.M.; Augland, L.E.; Lenz, O.; Bieg, G.; Haugen, T.; Grundvåg, S.A.; Jelby, M.E.; Midtkandal, I.; Dolezych, M.; Hjálmarsdóttir, H.R. Sylfjellet: A new outcrop of the Paleogene Van Mijenfjorden Group in Svalbard. *arktos* **2020**, *6*, 17–38. [CrossRef]
31. Dypvik, H.; Riber, L.; Burca, F.; Rüther, D.; Jargvoll, D.; Nagy, J.; Jochmann, M. The Paleocene–Eocene thermal maximum (PETM) in Svalbard—Clay mineral and geochemical signals. *Palaeogeogr. Palaeoclimatol. Palaeoecol.* **2011**, *302*, 156–169. [CrossRef]
32. Doerner, M.; Berner, U.; Erdmann, M.; Barth, T. Geochemical characterization of the depositional environment of Paleocene and Eocene sediments of the Tertiary Central Basin of Svalbard. *Chem. Geol.* **2020**, *542*, 119587. [CrossRef]
33. Smelror, M.; Larssen, G.B. Are there Upper Cretaceous sedimentary rocks preserved on Sørkapp land, Svalbard? *Norw. J. Geol.* **2016**, *96*, 147–158. [CrossRef]
34. Gilmullina, A.; Klausen, T.G.; Doré, A.G.; Sirevaag, H.; Suslova, A.; Eide, C.H. Arctic sediment routing during the Triassic: Sinking the Arctic Atlantis. *J. Geol. Soc.* **2023**, *180*, jgs2022-2018. [CrossRef]
35. Plink-Björklund, P.; Mellere, D.; Steel, R.J. Turbidite variability and architecture of sand-prone, deep-water slopes: Eocene clinoforms in the central basin, spitsbergen. *J. Sediment. Res.* **2001**, *71*, 895–912. [CrossRef]
36. Charles, A.J.; Condon, D.J.; Harding, I.C.; Pälike, H.; Marshall, J.E.A.; Cui, Y.; Kump, L.; Croudace, I.W. Constraints on the numerical age of the Paleocene-Eocene boundary. *Geochem. Geophys. Geosystems* **2011**, *12*, Q0AA17. [CrossRef]
37. Critelli, S.; Reed, W.E. Provenance and stratigraphy of the Devonian (Old Red Sandstone) and Carboniferous sandstones of Spitsbergen, Svalbard. *Eur. J. Mineral. -Ohne Beih.* **1999**, *11*, 149–166. [CrossRef]
38. Dallmeyer, R.D.; Peucat, J.J.; Hirajima, T.; Ohta, Y. Tectonothermal chronology within a blueschist-eclogite complex, west-central Spitsbergen, Svalbard: Evidence from 40Ar39Ar and RbSr mineral ages. *Lithos* **1990**, *24*, 291–304. [CrossRef]
39. Pettersson, C.H.; Tebenkov, A.M.; Larionov, A.N.; Andresen, A.; Pease, V. Timing of migmatization and granite genesis in the Northwestern Terrane of Svalbard, Norway: Implications for regional correlations in the Arctic Caledonides. *J. Geol. Soc.* **2009**, *166*, 147–158. [CrossRef]
40. Kośmińska, K.; Spear, F.S.; Majka, J.; Faehnrich, K.; Manecki, M.; Piepjohn, K.; Dallmann, W.K. Deciphering late Devonian–early Carboniferous P–T–t path of mylonitized garnet-mica schists from Prins Karls Forland, Svalbard. *J. Metamorph. Geol.* **2020**, *38*, 471–493. [CrossRef]
41. Nagy, J.; Kaminski, M.A.; Johnsen, K.; Mitlehner, A.G. Foraminiferal, palynomorph, and diatom biostratigraphy and paleoenvironments of the Torsk Formation: A reference section for the Paleocene-Eocene transition in the western Barents Sea. In *Contributions to the Micropaleontology and Paleoceanography of the Northern North Atlantic*; Hass, H.C., Kaminski, M.A., Eds.; Grzybowski Foundation Special Publication: Krakow, Poland, 1997; Volume 5, pp. 15–38.
42. Knutsen, S.M.; Skjold, L.J.; Skott, P.H. Palaeocene and Eocene development of the Tromso Basin-sedimentary response to rifting and early sea-floor spreading in the Barents Sea area. *Nor. Geol. Tidsskr.* **1992**, *72*, 191–207.

43. Grundvåg, S.A.; Marin, D.; Kairanov, B.; Śliwińska, K.K.; Nøhr-Hansen, H.; Jelby, M.E.; Escalona, A.; Olaussen, S. The Lower Cretaceous succession of the northwestern Barents Shelf: Onshore and offshore correlations. *Mar. Pet. Geol.* **2017**, *86*, 834–857. [CrossRef]
44. Midtkandal, I.; Faleide, J.I.; Faleide, T.S.; Serck, C.S.; Planke, S.; Corseri, R.; Dimitriou, M.; Nystuen, J.P. Lower Cretaceous Barents Sea strata: Epicontinental basin configuration, timing, correlation and depositional dynamics. *Geol. Mag.* **2020**, *157*, 458–476. [CrossRef]
45. Klausen, T.G.; Müller, R.; Slama, J.; Helland-Hansen, W. Evidence for late triassic provenance areas and Early Jurassic sediment supply turnover in the Barents Sea Basin of Northern Pangea. *Lithosphere* **2017**, *9*, 14–28. [CrossRef]
46. Klausen, T.G.; Müller, R.; Sláma, J.; Olaussen, S.; Rismyhr, B.; Helland-Hansen, W. Depositional history of a condensed shallow marine reservoir succession: Stratigraphy and detrital zircon geochronology of the Jurassic Stø Formation, Barents Sea. *J. Geol. Soc.* **2018**, *175*, 130–145. [CrossRef]
47. Fleming, E.J.; Flowerdew, M.J.; Smyth, H.R.; Scott, R.A.; Morton, A.C.; Omma, J.E.; Frei, D.; Whitehouse, M.J. Provenance of Triassic sandstones on the southwest Barents Shelf and the implication for sediment dispersal patterns in northwest Pangaea. *Mar. Pet. Geol.* **2016**, *78*, 516–535. [CrossRef]
48. Line, L.H.; Müller, R.; Klausen, T.G.; Jahren, J.; Hellevang, H. Distinct petrographic responses to basin reorganization across the Triassic–Jurassic boundary in the southwestern Barents Sea. *Basin Res.* **2020**, *32*, 1463–1484. [CrossRef]
49. Senger, K.; Brugmans, P.; Grundvåg, S.-A.; Jochmann, M.M.; Nøttvedt, A.; Olaussen, S.; Skotte, A.; Smyrak-Sikora, A. Petroleum, coal and research drilling onshore Svalbard: A historical perspective. *Nor. J. Geol.* **2019**, *99*, Nr 3. [CrossRef]
50. Gabrielsen, R.H.; Frerseth, R.B.; Jensen, L.N.; Kalheim, J.E.; Riis, F. Structural elements of the Norwegian continental shelf. *Nor. Pet. Dir. Bull.* **1990**, *6*, 33p.
51. Omosanya, K.O.; Harishidayat, D.; Marheni, L.; Johansen, S.E.; Felix, M.; Abrahamson, P. Recurrent mass-wasting in the Sørvestsnaget Basin Southwestern Barents Sea: A test of multiple hypotheses. *Mar. Geol.* **2016**, *376*, 175–193. [CrossRef]
52. Suttner, L.J.; Basu, A.; Ingersoll, R.V.; Bullard, T.F.; Ford, R.L.; Pickle, J.D. The effect of grain size on detrital modes; a test of the Gazzi-Dickinson point-counting method; discussion and reply. *J. Sediment. Res.* **1985**, *55*, 616–618. [CrossRef]
53. Folk, R.L.; Andrews, P.B.; Lewis, D.W. Detrital sedimentary rock classification and nomenclature for use in New-Zealand. *N. Z. J. Geol. Geophys.* **1970**, *13*, 937–968. [CrossRef]
54. Morton, A.C.; Hallsworth, C. Identifying provenance-specific features of detrital heavy mineral assemblages in sandstones. *J. Sediment. Geol.* **1994**, *90*, 241–256. [CrossRef]
55. Tyrrell, S.; Haughton, P.D.W.; Daly, J.S.; Kokfelt, T.F.; Gagnevin, D. The use of the common Pb isotope composition of detrital K-feldspar grains as a provenance tool and its application to Upper Carboniferous paleodrainage, northern England. *J. Sediment. Res.* **2006**, *76*, 324–345. [CrossRef]
56. Flowerdew, M.J.; Tyrrell, S.; Riley, T.R.; Whitehouse, M.J.; Mulvaney, R.; Leat, P.T.; Marschall, H.R. Distinguishing East and West Antarctic sediment sources using the Pb isotope composition of detrital K-feldspar. *Chem. Geol.* **2012**, *292*, 88–102. [CrossRef]
57. Chew, D.M.; Petrus, J.A.; Kamber, B.S. U-Pb LA-ICPMS dating using accessory mineral standards with variable common Pb. *Chem. Geol.* **2014**, *363*, 185–199. [CrossRef]
58. Chew, D.M.; Sylvester, P.J.; Tubrett, M.N. U-Pb and Th-Pb dating of apatite by LA-ICPMS. *Chem. Geol.* **2011**, *280*, 200–216. [CrossRef]
59. Stacey, J.S.; Kramers, J.D. Approximation of terrestrial lead isotope evolution by a two-stage model. *Earth Planet Sc. Lett.* **1975**, *26*, 207–221. [CrossRef]
60. Wiedenbeck, M.; Alle, P.; Corfu, F.; Griffin, W.L.; Meier, M.; Oberli, F.; Vonquadt, A.; Roddick, J.C.; Speigel, W. 3 Natural Zircon Standards for U-Th-Pb, Lu-Hf, Trace-Element and Ree Analyses. *Geostand. Newslett.* **1995**, *19*, 1–23. [CrossRef]
61. Sláma, J.; Košler, J.; Condon, D.J.; Crowley, J.L.; Gerdes, A.; Hanchar, J.M.; Horstwood, M.S.A.; Morris, G.A.; Nasdala, L.; Norberg, N.; et al. Plešovice zircon-A new natural reference material for U-Pb and Hf isotopic microanalysis. *Chem Geol* **2008**, *249*, 1–35. [CrossRef]
62. Black, L.P.; Kamo, S.L.; Allen, C.M.; Davis, D.W.; Aleinikoff, J.N.; Valley, J.W.; Mundil, R.; Campbell, I.H.; Korsch, R.J.; Williams, I.S.; et al. Improved 206Pb/238U microprobe geochronology by the monitoring of a trace-element-related matrix effect; SHRIMP, ID-TIMS, ELA-ICP-MS and oxygen isotope documentation for a series of zircon standards. *Chem. Geol.* **2004**, *205*, 115–140. [CrossRef]
63. Luvizotto, G.L.; Zack, T.; Meyer, H.P.; Ludwig, T.; Triebold, S.; Kronz, A.; Münker, C.; Stockli, D.F.; Prowatke, S.; Klemme, S.; et al. Rutile crystals as potential trace element and isotope mineral standards for microanalysis. *Chem. Geol.* **2009**, *261*, 346–369. [CrossRef]
64. Zack, T.; Stockli, D.F.; Luvizotto, G.L.; Barth, M.G.; Belousova, E.; Wolfe, M.R.; Hinton, R.W. In situ U-Pb rutile dating by LA-ICP-MS: 208Pb correction and prospects for geological applications. *Contrib. Miner. Petr.* **2011**, *162*, 515–530. [CrossRef]
65. Cochrane, R.; Spikings, R.A.; Chew, D.; Wotzlaw, J.F.; Chiaradia, M.; Tyrrell, S.; Schaltegger, U.; Van der Lelij, R. High temperature (>350 °C) thermochronology and mechanisms of Pb loss in apatite. *Geochim. Cosmochim. Ac.* **2014**, *127*, 39–56. [CrossRef]
66. Thomson, S.N.; Gehrels, G.E.; Ruiz, J.; Buchwaldt, R. Routine low-damage apatite U-Pb dating using laser ablation-multicollector-ICPMS. *Geochem. Geophys. Geosystems* **2012**, *13*, Q0AA21. [CrossRef]

67. Krestianinov, E.; Amelin, Y.; Neymark, L.A.; Aleinikoff, J.N. U-Pb systematics of uranium-rich apatite from Adirondacks: Inferences about regional geological and geochemical evolution, and evaluation of apatite reference materials for in situ dating. *Chem. Geol.* **2021**, *581*, 120417. [CrossRef]
68. Paul, A.N.; Spikings, R.A.; Gaynor, S.P. U-Pb ID-TIMS reference ages and initial Pb isotope compositions for Durango and Wilberforce apatites. *Chem. Geol.* **2021**, *586*, 120604. [CrossRef]
69. Frei, D.; Gerdes, A. Precise and accurate in situ U-Pb dating of zircon with high sample throughput by automated LA-SF-ICP-MS. *Chem. Geol.* **2009**, *261*, 261–270. [CrossRef]
70. Jackson, S.E.; Pearson, N.J.; Griffin, W.L.; Belousova, E.A. The application of laser ablation-inductively coupled plasma-mass spectrometry to in situ U-Pb zircon geochronology. *Chem. Geol.* **2004**, *211*, 47–69. [CrossRef]
71. Nasdala, L.; Corfu, F.; Valley, J.W.; Spicuzza, M.J.; Wu, F.-Y.; Li, Q.-L.; Yang, Y.-H.; Fisher, C.; Münker, C.; Kennedy, A.K.; et al. Zircon M127–A Homogeneous Reference Material for SIMS U–Pb Geochronology Combined with Hafnium, Oxygen and, Potentially, Lithium Isotope Analysis. *Geostand. Geoanal. Res.* **2016**, *40*, 457–475. [CrossRef]
72. Schmitt, A.K.; Zack, T. High-sensitivity U-Pb rutile dating by secondary ion mass spectrometry (SIMS) with an O 2 + primary beam. *Chem. Geol.* **2012**, *332–333*, 65–73. [CrossRef]
73. Whitehouse, M.J.; Kamber, B.S. Assigning dates to thin gneissic veins in high-grade metamorphic terranes: A cautionary tale from Akilia, southwest Greenland. *J. Pet.* **2005**, *46*, 291–318. [CrossRef]
74. Riley, T.R.; Flowerdew, M.J.; Millar, I.L.; Whitehouse, M.J. Triassic magmatism and metamorphism in the Antarctic Peninsula: Identifying the extent and timing of the Peninsula Orogeny. *J. South Am. Earth Sci.* **2020**, *103*, 102732. [CrossRef]
75. Jeon, H.; Whitehouse, M.J. A Critical Evaluation of U–Pb Calibration Schemes Used in SIMS Zircon Geochronology. *Geostand. Geoanal. Res.* **2015**, *39*, 443–452. [CrossRef]
76. Nasdala, L.; Hofmeister, W.; Norberg, N.; Martinson, J.M.; Corfu, F.; Dörr, W.; Kamo, S.L.; Kennedy, A.K.; Kronz, A.; Reiners, P.W.; et al. Zircon M257-A homogeneous natural reference material for the ion microprobe U-Pb analysis of zircon. *Geostand. Geoanal. Res.* **2008**, *32*, 247–265. [CrossRef]
77. Meinhold, G. Rutile and its applications in earth sciences. *Earth-Sci. Rev.* **2010**, *102*, 1–28. [CrossRef]
78. Watson, E.B.; Wark, D.A.; Thomas, J.B. Crystallization thermometers for zircon and rutile. *Contrib. Miner. Petr.* **2006**, *151*, 413–433. [CrossRef]
79. Morton, A.C.; Yaxley, G. Detrital apatite geochemistry and its application in provenance studies. In *Sedimentary Provenance and Petrogenesis: Perspectives from Petrography and Geochemistry*; Geological Society of America: Boulder, CO, USA, 2007; Volume 420, pp. 319–344.
80. O'Sullivan, G.; Chew, D.; Kenny, G.; Henrichs, I.; Mulligan, D. The trace element composition of apatite and its application to detrital provenance studies. *Earth-Sci. Rev.* **2020**, *201*, 103044. [CrossRef]
81. Johansson, Å.; Gee, D.G.; Björklund, L.; Witt-Nilsson, P. Isotope studies of granitoids from the Bangenhuk Formation, Ny Friesland Caledonides, Svalbard. *Geol. Mag.* **1995**, *132*, 303–320. [CrossRef]
82. Johansson, Å.; Larionov, A.N.; Tebenkov, A.M.; Ohta, Y.; Gee, D.G. Caledonian granites of western and central Nordaustlandet, northeast Svalbard. *Gff* **2002**, *124*, 135–148. [CrossRef]
83. Slagstad, T.; Kirkland, C.L. The use of detrital zircon data in terrane analysis: A nonunique answer to provenance and tectonostratigraphic position in the Scandinavian Caledonides. *Lithosphere* **2017**, *9*, 1002–1011. [CrossRef]
84. Higgins, A.K.; Soper, N.J.; Leslie, A.G. The Ellesmerian and Caledonian orogenic belts of Greenland. *Polarforschung* **2000**, *68*, 141–151.
85. Nielsen, M.L.; Lee, M.; Ng, H.C.; Rushton, J.C.; Hendry, K.R.; Kihm, J.-H.; Nielsen, A.T.; Park, T.-Y.S.; Vinther, J.; Wilby, P.R. Metamorphism obscures primary taphonomic pathways in the early Cambrian Sirius Passet Lagerstätte, North Greenland. *Geology* **2021**, *50*, 4–9. [CrossRef]
86. Tegner, C.; Storey, M.; Holm, P.M.; Thorarinsson, S.B.; Zhao, X.; Lo, C.H.; Knudsen, M.F. Magmatism and Eurekan deformation in the High Arctic Large Igneous Province: 40Ar–39Ar age of Kap Washington Group volcanics, North Greenland. *Earth Planet Sc. Lett.* **2011**, *303*, 203–214. [CrossRef]
87. Barnes, C.J.; Walczak, K.; Janots, E.; Schneider, D.; Majka, J. Timing of Paleozoic Exhumation and Deformation of the High-Pressure Vestgötabreen Complex at the Motalafjella Nunatak, Svalbard. *Minerals* **2020**, *10*, 125. [CrossRef]
88. Manby, G.M. A reappraisal of chloritoid-bearing phyllites in the Forland Complex rocks of Prins Karls Forland, Spitsbergen. *Miner. Mag.* **1983**, *47*, 311–318. [CrossRef]
89. Majka, J.; Kośmińska, K. Magmatic and metamorphic events recorded within the Southwestern Basement Province of Svalbard. *arktos* **2017**, *3*, 5. [CrossRef]
90. Gasser, D.; Andresen, A. Caledonian terrane amalgamation of Svalbard: Detrital zircon provenance of mesoproterozoic to carboniferous strata from oscar II Land, western spitsbergen. *Geol. Mag.* **2013**, *150*, 1103–1126. [CrossRef]
91. Pettersson, C.H.; Pease, V.; Frei, D. U-Pb zircon provenance of metasedimentary basement of the Northwestern Terrane, Svalbard: Implications for the Grenvillian-Sveconorwegian orogeny and development of Rodinia. *Precambrian Res.* **2009**, *175*, 206–220. [CrossRef]
92. Vermeesch, P. Multi-sample comparison of detrital age distributions. *Chem. Geol.* **2013**, *341*, 140–146. [CrossRef]
93. Vermeesch, P.; Resentini, A.; Garzanti, E. An R package for statistical provenance analysis. *J. Sediment. Geol.* **2016**, *336*, 14–25. [CrossRef]

94. Røhr, T.S.; Andersen, T.; Dypvik, H. Provenance of Lower Cretaceous sediments in the Wandel Sea Basin, North Greenland. *J. Geol. Soc.* **2008**, *165*, 755–767. [CrossRef]
95. Czarniecka, U.; Haile, B.G.; Braathen, A.; Krajewski, K.P.; Kristoffersen, M.; Jokubauskas, P. Petrography, bulk-rock geochemistry, detrital zircon U–Pb geochronology and Hf isotope analysis for constraining provenance: An example from Middle Triassic deposits (Bravaisberget Formation), Sørkappøya, Svalbard. *Norw. J. Geol.* **2020**, *100*, 202017. [CrossRef]
96. Kirkland, C.L.; Pease, V.; Whitehouse, M.J.; Ineson, J.R. Provenance record from Mesoproterozoic-Cambrian sediments of Peary Land, North Greenland: Implications for the ice-covered Greenland Shield and Laurentian palaeogeography. *Precambrian Res.* **2009**, *170*, 43–60. [CrossRef]
97. Pózer Bue, E.; Andresen, A. Constraining depositional models in the Barents Sea region using detrital zircon U–Pb data from Mesozoic sediments in Svalbard. *Geol. Soc. Lond. Spec. Publ.* **2014**, *386*, 261–279. [CrossRef]
98. Morris, G.A.; Kirkland, C.L.; Pease, V. Orogenic paleofluid flow recorded by discordant detrital zircons in the Caledonian foreland basin of northern Greenland. *Lithosphere* **2015**, *7*, 138–143. [CrossRef]
99. Andresen, A.; Agyei-Dwarko, N.Y.; Kristoffersen, M.; Hanken, N.M. A Timanian foreland basin setting for the late Neoproterozoic-early Palaeozoic cover sequences (Dividal Group) of Northeastern Baltica. *Geol. Soc. Spec. Publ.* **2014**, *390*, 157–175. [CrossRef]
100. Zhang, W.; Roberts, D.; Pease, V. Provenance characteristics and regional implications of Neoproterozoic, Timanian-margin successions and a basal Caledonian nappe in northern Norway. *Precambrian Res.* **2015**, *268*, 153–167. [CrossRef]
101. Lorenz, H.; Gee, D.G.; Korago, E.; Kovaleva, G.; McClelland, W.C.; Gilotti, J.A.; Frei, D. Detrital zircon geochronology of Palaeozoic Novaya Zemlya-a key to understanding the basement of the Barents Shelf. *Terra Nova* **2013**, *25*, 496–503. [CrossRef]
102. Pease, V.; Scott, R.A. Crustal affinities in the Arctic Uralides, northern Russia: Significance of detrital zircon ages from Neoproterozoic and Palaeozoic sediments in Novaya Zemlya and Taimyr. *J. Geol. Soc.* **2009**, *166*, 517–527. [CrossRef]
103. Pettersson, C.H.; Pease, V.; Frei, D. Detrital zircon U-Pb ages of Silurian-Devonian sediments from NW Svalbard: A fragment of Avalonia and Laurentia? *J. Geol. Soc.* **2010**, *167*, 1019–1032. [CrossRef]
104. Beranek, L.P.; Gee, D.G.; Fisher, C.M. Detrital zircon U-Pb-Hf isotope signatures of Old Red Sandstone strata constrain the Silurian to Devonian paleogeography, tectonics, and crustal evolution of the Svalbard Caledonides. *GSA Bull.* **2020**, *132*, 1987–2003. [CrossRef]
105. Andreichev, V.L.; Soboleva, A.A.; Gehrels, G. U-Pb dating and provenance of detrital zircons from the Upper Precambrian deposits of North Timan. *Stratigr. Geol. Correl.* **2014**, *22*, 147–159. [CrossRef]
106. Kirkland, C.L.; Daly, J.S.; Eide, E.A.; Whitehouse, M.J. Tectonic evolution of the Arctic Norwegian Caledonides from a texturally- and structurally-constrained multi-isotopic (Ar-Ar, Rb-Sr, Sm-Nd, U-Pb) study. *Am. J. Sci.* **2007**, *307*, 459–526. [CrossRef]
107. Kirkland, C.L.; Daly, J.S.; Whitehouse, M.J. Basement-cover relationships of the Kalak Nappe Complex, Arctic Norwegian Caledonides and constraints on neoproterozoic terrane assembly in the North Atlantic Region. *Precambrian Res.* **2008**, *160*, 245–276. [CrossRef]
108. Kirkland, C.L.; Bingen, B.; Whitehouse, M.J.; Beyer, E.; Griffin, W.L. Neoproterozoic palaeogeography in the North Atlantic Region: Inferences from the Akkajaure and Seve Nappes of the Scandinavian Caledonides. *Precambrian Res.* **2011**, *186*, 127–146. [CrossRef]
109. Nutman, A.P.; Dawes, P.R.; Kalsbeek, F.; Hamilton, M.A. Palaeoproterozoic and Archaean gneiss complexes in northern Greenland: Palaeoproterozoic terrane assembly in the High Arctic. *Precambrian Res.* **2008**, *161*, 419–451. [CrossRef]
110. Khudoley, A.K.; Sobolev, N.N.; Petrov, E.O.; Ershova, V.B.; Makariev, A.A.; Makarieva, E.V.; Gaina, C.; Sobolev, P.O. A reconnaissance provenance study of Triassic–Jurassic clastic rocks of the Russian Barents Sea. *Gff* **2019**, *141*, 263–271. [CrossRef]
111. Soloviev, A.V.; Zaionchek, A.V.; Suprunenko, O.I.; Brekke, H.; Faleide, J.I.; Rozhkova, D.V.; Khisamutdinova, A.I.; Stolbov, N.M.; Hourigan, J.K. Evolution of the provenances of Triassic rocks in Franz Josef Land: U/Pb LA-ICP-MS dating of the detrital zircon from Well Severnaya. *Lithol. Miner. Resoure* **2015**, *50*, 102–116. [CrossRef]
112. Kruskal, J.B. Multidimensional scaling by optimizing goodness of fit to a nonmetric hypothesis. *Psychometrika* **1964**, *29*, 1–27. [CrossRef]
113. Bjerager, M.; Alsen, P.; Hovikoski, J.; LINDSTRÖM, S.; Pilgaard, A.; Stemmerik, L.; Therkelsen, J. Triassic lithostratigraphy of the Wandel Sea Basin, North Greenland. *Bull. Geol. Soc. Den.* **2019**, *67*, 83–105.
114. Gilmullina, A.; Klausen, T.G.; Doré, A.G.; Rossi, V.M.; Suslova, A.; Eide, C.H. Linking sediment supply variations and tectonic evolution in deep time, source-to-sink systems—The Triassic Greater Barents Sea Basin. *GSA Bull.* **2021**, *134*, 1760–1780. [CrossRef]
115. Boyden, J.A.; Müller, R.D.; Gurnis, M.; Torsvik, T.H.; Clark, J.A.; Turner, M.; Ivey-Law, H.; Watson, R.J.; Cannon, J.S. Next-generation plate-tectonic reconstructions using GPlates. In *Geoinformatics: Cyberinfrastructure for the Solid Earth Sciences*; Cambridge University Press: Cambridge, UK, 2011; pp. 95–114.
116. Petersen, T.G.; Hamann, N.E.; Stemmerik, L. Correlation of the Palaeogene successions on the north-east Greenland and Barents Sea margins. *Bull. Geol. Soc. Den.* **2016**, *64*, 77–96.
117. Lasabuda, A.P.; Johansen, N.S.; Laberg, J.S.; Faleide, J.I.; Senger, K.; Rydningen, T.A.; Patton, H.; Knutsen, S.-M.; Hanssen, A. Cenozoic uplift and erosion of the Norwegian Barents Shelf–A review. *Earth-Sci. Rev.* **2021**, *217*, 103609. [CrossRef]